TRANSPORT OF AIR PLASMAS

Grant No. F49620-94-1-0052

Final Technical Report
Prepared for Dr. Robert J. Barker
Air Force Office of Scientific Research

For the Period
November 15, 1993 to August 31, 1997

Submitted by

Professor Charles H. Kruger
Principal Investigator

November 1997

HIGH TEMPERATURE GASDYNAMICS LABORATORY
Mechanical Engineering Department
Stanford University

REPORT DOCUMENTATION PAGE

Form Approved
OMB No. 0704-0188

1. AGENCY USE ONLY (*Leave Blank*)	2. REPORT DATE	3. REPORT TYPE AND DATES COVERED
	15 Nov 97	**Final Technical Report for the period 15 Nov 93 - 31 Aug 97**

4. TITLE AND SUBTITLE
Transport of Air Plasmas

5. FUNDING NUMBERS
G: F49620-94-1-0052
PR: 2301
TA: ES

6. AUTHORS
Charles H. Kruger, P.I.
Christophe O. Laux
Richard J. Gessman

7. PERFORMING ORGANIZATION NAME(S) AND ADDRESS(ES)
Stanford University
Thermosciences Division
Department of Mechanical Engineering
Stanford, CA 94305-3030

8. PERFORMING ORGANIZATION REPORT NUMBER

9. SPONSORING / MONITORING AGENCY NAME(S) AND ADDRESS(ES)
AFOSR/NE
Dr. Robert J. Barker (202) 767-5011
110 Duncan Avenue Suite B115
Bolling AFB DC 20332-0001

10. SPONSORING / MONITORING AGENCY REPORT NUMBER

11. SUPPLEMENTARY NOTES

12a. DISTRIBUTION / AVAILABILITY STATEMENT
'A'

12b. DISTRIBUTION CODE

13. ABSTRACT *(Maximum 200 words)*

This report describes research results on the Transport of Air Plasmas obtained in the High Temperature Gasdynamics Laboratory at Stanford University. This research has emphasized studies of ionizational nonequilibrium and electron recombination in atmospheric pressure air plasmas. The present report discusses, in the first part, theoretical investigations of the mechanism for ionizational nonequilibrium and, in the second part, measurements of the rate of recombination of electrons in air, nitrogen, and air/argon plasmas. These investigations have shown the surprising result that ionizational nonequilibrium in air (or nitrogen) plasmas results from and is controlled by the chemistry of neutral species. It was also found that very large discrepancies exist between the rates proposed in the literature for the controlling reactions. The experimental results have confirmed the proposed recombination mechanism and have provided an assessment of the rates of the controlling reactions, namely N + O + M ⇔ NO + M in air plasmas, and N + N + M ⇔ N2 + M in nitrogen plasmas. Novel diagnostic techniques were developed for this work, in particular for the measurement of electron number densities between 10^{11} and 10^{13} /cc using the optical radiation emitted by the predissociative delta (C-X) bands of NO.

14. **SUBJECT TERMS**
Air Plasmas, Nitrogen Plasmas, Argon Plasmas,
Optical Emission Spectroscopy, Optical Diagnostics, Electron Number Densities
Ionizational Nonequilibrium, Electron Recombination, Chemical Kinetics

15. NUMBER OF PAGES
45

16. PRICE CODE

17. SECURITY CLASSIFICATION OF REPORT	18. SECURITY CLASSIFICATION OF THIS PAGE	19. SECURITY CLASSIFICATION OF ABSTRACT	20. LIMITATION OF ABSTRACT
Unclassified	**Unclassified**	**Unclassified**	**UL**

1. Contents

Section **Page**

2. Introduction

This report is the final report on the research program on the transport of air plasmas conducted in the High Temperature Gasdynamics Laboratory at Stanford University. This research was supported by a grant from the Air Force Office of Scientific Research (Grant No. F49620-94-1-0052) with Dr. Robert J. Barker as Technical Monitor, and was conducted under the direction of Professor Charles H. Kruger. Under this program, two students have received their M.S. degree, and one graduate student is about to complete his Ph.D. One Research Associate, Dr. Christophe O. Laux, has also been involved in this program.

This program is intended to explore the feasibility of transporting an atmospheric pressure air plasma with a residence time of a few milliseconds while maintaining an electron density greater than 10^{13} cm^{-3} between the plasma source and the destination volume of interest. Atmospheric pressure plasmas are typically "thermal," meaning that electrons and heavy particles have the same kinetic temperature, and that this temperature is also equal to the vibrational and rotational temperatures. Equilibration of the kinetic temperatures is a consequence of relatively high electron number densities, frequent collisions between charged and neutral particles, and large Coulomb cross sections for collisions between charged particles. However, when the plasma is forced to recombine at a fast rate, both chemical and ionizational nonequilibrium can occur owing to finite recombination rates for atoms, ions and electrons. In particular, electron densities are driven out of equilibrium with respect to ground-state populations. In this case, strong coupling between the populations of bound electronic states and the electron density can have major effects on the recombination rate itself, on chemical reactions in general, on the local emission of radiation, and on the utility of standard emission diagnostics. Effects on the overall energy balance and fluid mechanics include nonequilibrium radiation losses, recombination energy release, and variations in the thermal or electrical conductivity.

When an electrical discharge is used to create high electron number densities in an atmospheric pressure air flow at temperatures of about 1000 K, the thermodynamic state of the plasma can be characterized by a situation intermediary between the two following cases. In the first limiting case, the kinetic temperatures of electrons and heavy species after the discharge remain equal to 1000 K; a higher number density of electrons (and ions for charge balance) is produced, but the concentrations of neutral species are unchanged. In the second limiting case, the temperatures of the gas and of the electrons both increase, and the concentrations of charged and neutral species correspond to chemical equilibrium at the higher temperature; for sake of argument, let us assume in the latter case that the discharge increases the electron number density to a value of approximately 2×10^{15} cm^{-3} (which in chemical equilibrium air corresponds to ~6500 K).

The kinetics of electron recombination after the discharge can be examined in these two cases by means of three reaction mechanisms proposed in the literature (Dunn and Kang,[1] Gupta et al.,[2] and Park[3,4]) using a methodology that will be discussed in more details in Sections 3 and 4 of this report. In the first case, the temperature is assumed to remain constant at 1000 K, and the plasma is allowed to recombine over a period of 1 msec. In the second case, the temperature is assumed to drop linearly with time, from 6500 K to 1000 K, within a duration of 1 msec. From the resulting electron number density variations shown in Figs. 1 and 2, it can be observed that in both cases the predicted electron densities at 1 msec. are greater than equilibrium densities by large factors (there would be virtually no electrons in chemical equilibrium air at 1000 K). Moreover, it can be seen from the figures that the two cases present notable similarities in the large differences (up to a factor of 50) resulting from the three reaction mechanisms at 1 msec. While in the first case electron recombination is completely controlled by the dissociative recombination reaction $NO^+ + e^- \Leftrightarrow N + O$, it will be shown in this report that a more complex situation arises in the second case. Since the conditions prevailing after a real discharge are expected to fall between these two extreme cases, it is important to determine which reactions control electron recombination and to provide accurate rates for these reactions.

In this research program, we have followed a dual theoretical and experimental approach. The first part of the effort was to investigate theoretically the kinetics of electron recombination in air plasmas, using the three reaction mechanisms[1-4] mentioned earlier, in order to determine which reactions control electron recombination. As will be seen Section 3, this analysis has shown that the rates of recombination of neutral species govern to a large extent the rates of recombination of electrons and charged species. Moreover, this analysis has uncovered large discrepancies between the rate coefficients of the various mechanisms. To assess the quality of the various reaction mechanisms and establish more accurate reaction rates for those reactions found to play a major role on electron recombination, experiments have been conducted with thermal, atmospheric pressure plasmas (air, nitrogen, and air/argon) produced with an inductively coupled plasma torch and transported within a well-controlled flow environment. Several plasma reactors have been built to create experimental conditions corresponding to an ionizational nonequilibrium situation similar to that investigated theoretically. Section 4 of this report describes the experimental results obtained with these plasma mixtures, and how these results were used to assess the various reaction mechanisms and the rate coefficients for critical reactions controlling ionizational nonequilibrium. Publications and presentations resulting from or related to this work are cited in Section 5, and Section 6 lists the personnel who contributed to this research.

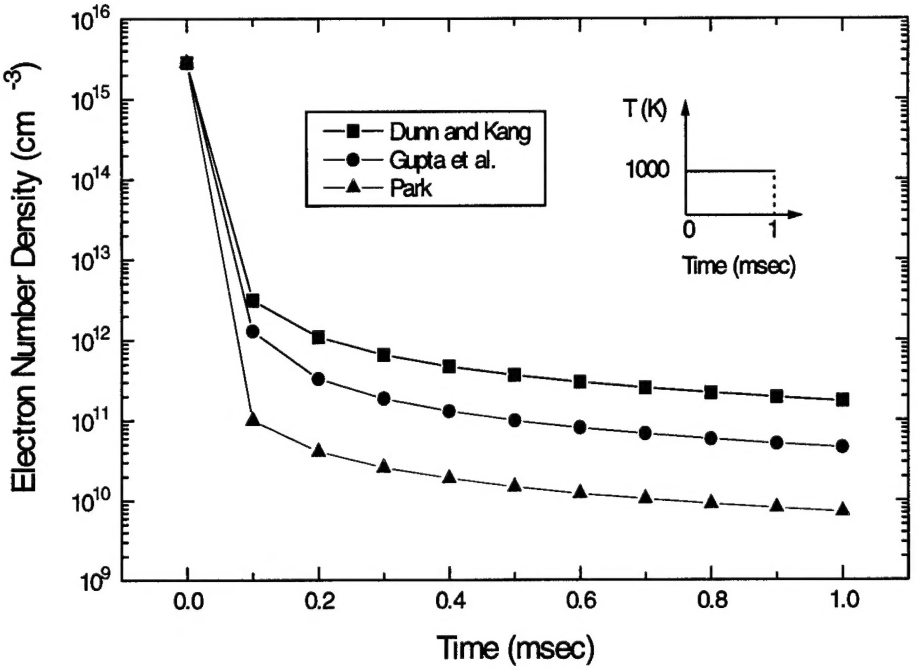

Figure 1. Electron recombination in a thermal plasma at 1000 K.

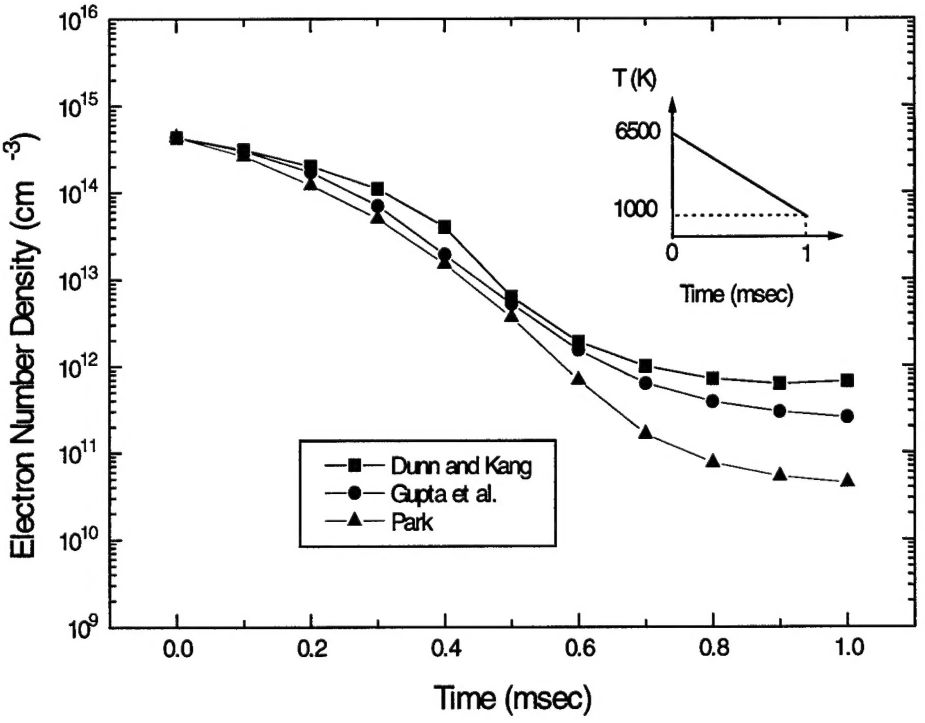

Figure 2. Electron recombination in a thermal plasma with temperature decreasing linearly from 6500 to 1000 K.

3. Recombination mechanism of nonequilibrium air plasmas: theoretical results.

This section describes theoretical investigations of plasma kinetics in a recombining air plasma assumed to be thermal (equal electron and heavy particle temperatures). While the phenomena described herein are by no means limited to thermal plasmas, they can be described more clearly with a single temperature plasma. The CHEMKIN solver[5] was used for one-dimensional kinetics modeling with specified initial concentrations and with imposed temperature variations. Three air reaction mechanisms (Dunn and Kang,[1] Gupta et al.,[2] and Park[3,4]) were considered. Reverse reaction rates were obtained by detailed balance using the equilibrium thermodynamic properties computed by Liu and Vinokur.[6] The air plasma was assumed to be initially in chemical equilibrium at 7500 K and 1 atm. A linear temperature drop from 7500 to 4500 K within a duration of 0.6 ms was then imposed to the plasma, and the concentration evolution of the major neutral and charged species was computed with CHEMKIN. At each time, concentrations were normalized to their chemical equilibrium values at the corresponding temperature. The resulting normalized concentrations, or nonequilibrium factors, are shown in Fig. 3. Observations derived from these results are discussed in Sections 3.1-3.3.

To check the thermal plasma assumption, we have calculated the differences between the electron kinetic temperature T_e, the gas kinetic temperature T_h, and the vibrational temperature T_v and found that they are negligible for the present conditions. For molecular plasmas with no applied external field, the electron energy equation is:[7]

$$3n_e\left(\sum_{species\ s}\frac{m_e}{m_s}\bar{\nu}_{es}\delta_s k(T_e-T_h)\right)=\sum_{ion\ i}\varepsilon_i\left.\frac{\partial n_i}{\partial t}\right|_{3\ body-recombination}, \qquad (1)$$

where n_e, m_e, and m_s represent the electron number density, the electron mass, and the mass of heavy species s, respectively, δ_s is the so-called nonelastic energy loss factor, used as a multiplier to the rate of energy transferred by elastic collisions to model the effect of nonelastic collisions, and the term on the RHS represents the net rate of energy transferred to the electrons by three-body ion recombination reactions. (Note that the (exothermic) dissociative recombination reaction $NO^+ + e \Leftrightarrow N + O$, which is the principal electron recombination channel here, does not increase the electron temperature but instead the thermal energy of the gas.) Using the nonelastic energy loss factors of Ref. [8], Eqn. 1 predicts that, for all three reaction mechanisms, the differences between gas and electron kinetic temperatures are less than 25 K throughout the reaction zone. That the translational and vibrational modes of heavy particles are equilibrated can be shown in turn by comparing the characteristic flow time, 600 μsec here, to the slowest vibrational relaxation time of plasma species, 20 μsec here (since for the present conditions the slowest vibrational relaxation rate parameter $p_c\tau$ is 2×10^{-5} atm-sec [Ref. [3], p. 59]). As the flow time is more than 30 times greater than the vibrational time, it is clear that the translational and vibrational modes are equilibrated.

3.1. Mechanism of Dunn and Kang:

With this mechanism, CHEMKIN predicts (see Fig. 3) that O and N_2 remain essentially in equilibrium while N, O_2, and NO populations depart from equilibrium by one to two orders of magnitude. (Here, by equilibrium we mean that the concentrations at a given temperature and pressure are nearly equal to their global equilibrium values, not that O and N_2 are in equilibrium with O_2 and N, respectively.) Charged species populations also deviate from equilibrium. In particular, the electron overpopulation factor reaches approximately three at time t = 0.6 ms.

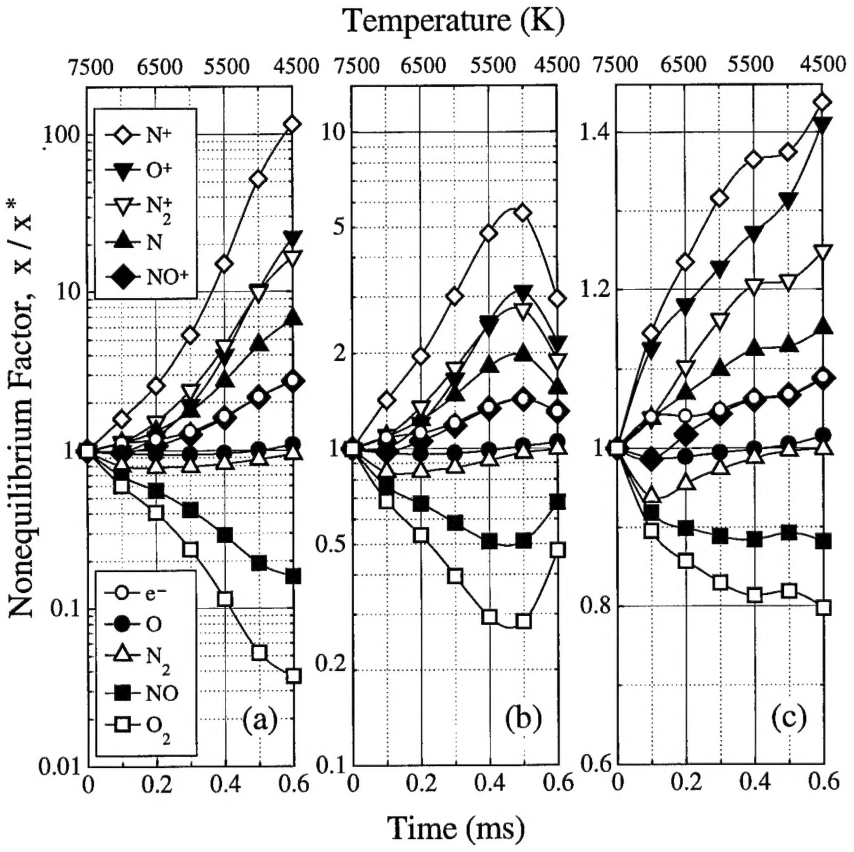

Figure 3. Nonequilibrium factors predicted with the reaction mechanisms of (a) Dunn and Kang, (b) Gupta, Yos, Thompson, and Lee, and (c) Park. The validity of Eqns. 2,4,5 for t > 0.3 ms can be verified from these figures. For instance, that the electron overpopulation factor varies as the square-root of the N-overpopulation factor (Eqn. 4) can be seen most easily in the logarithmic plots (3a and 3b) where the electron overpopulation curve lies half the distance from the equilibrium line (x/x* = 1) to the N-overpopulation curve.

To understand the process leading to ionizational nonequilibrium, it is instructive to examine the reaction rates. Listed in Table 1 for each reaction are the forward and reverse rates at t = 0.6 ms (T = 4500 K), as well as their differences. These differences represent the net rate of production/destruction of species by a given reaction and can be used to rank the reactions. Accordingly, the reactions in Table 1 are listed by order of

decreasing efficiency. The last column of the table contains for each reaction the ratio between the difference and the sum of the rates. When this ratio is close to zero, the reaction is equilibrated; a value close to unity indicates nonequilibrium. The analysis below is based on the inspection of the rates at 0.6 ms, but is equally valid at any prior time $t \geq 0.3$ ms.

Considered first is the chemistry of neutral species. Reactions (1-3) in Table 1 are the most efficient reactions, by at least one order of magnitude. Since their net rates are approximately equal, these reactions overall promote N recombination ($2N \rightarrow N_2$) while maintaining O, O_2, and NO close to quasi-steady state (QSS).[†] Therefore, for the conditions considered, only small concentration changes occur for O, O_2, and NO. Between 7500 and 4500 K, O-atoms represent between 99 and 90% of the oxygen-containing species and remain close to chemical equilibrium. In contrast, the populations of O_2 and NO are below their chemical equilibrium values because the mole fraction increases required to reach equilibrium at 4500 K from initially equilibrium at 7500 K, equal to 439 and 19, respectively, are too large to be compatible with approximate QSS. Finally, nitrogen recombination reactions are fast enough to maintain N_2 in equilibrium (only a factor 5 increase in N_2 mole fraction is necessary), but not to keep N itself in chemical equilibrium (a factor 91 mole fraction decrease would be required). Quantitatively, since N_2 and O are close to equilibrium and since reactions (1) and (2) are essentially equilibrated, we have:

$$\begin{aligned} [NO]/[NO]^* &\cong \left([N]/[N]^*\right)^{-1} \\ [O_2]/[O_2]^* &\cong \left([N]/[N]^*\right)^{-2} \end{aligned} , \tag{2}$$

where the asterisks denote equilibrium concentrations. Thus the chemistry of neutral species is controlled by N-atom recombination reactions.

Second, Table 1 shows that reaction 12 ($NO^+ + e \Leftrightarrow N + O$) is the main channel for electron recombination since its net rate is much greater than the rates of the other electron recombination reactions (19, 20, 23, 27-29). Also, it is equilibrated and therefore we have:

$$\frac{[NO^+][e^-]}{[N][O]} \cong \left(\frac{[NO^+][e^-]}{[N][O]}\right)^* . \tag{3}$$

[†] It is interesting to note that the Zel'dovich reactions (reactions 1 and 2 in Table 1) produce O and N_2 while maintaining NO in quasi-steady state. To readers more familiar with combustion environments where the endothermic $O + N_2 \rightarrow N + NO$ and exothermic $N + O_2 \rightarrow O + NO$ reactions combine to produce NO while N atoms remain in QSS, this may appear surprising. Here, the atypical behavior arises because the concentration of N atoms is much higher than in flames and thus causes reaction (1) to proceed from right to left, the opposite from combustion.

Noting that NO^+ is the major ion and that $[O] \cong [O]^*$, it follows that:

$$[e^-]/[e^-]^* \cong \sqrt{[N]/[N]^*} \cong [NO^+]/[NO^+]^* \tag{4}$$

Furthermore, since all charge-exchange (18, 22, 24, 25) and charge-transfer (26) reactions are close to equilibrium, the following relations are also verified:

$$\begin{aligned} [N^+]/[N^+]^* &\cong ([N]/[N]^*)^{5/2} \\ [O^+]/[O^+]^* &\cong ([N]/[N]^*)^{3/2} \\ [N_2^+]/[N_2^+]^* &\cong ([N]/[N]^*)^{3/2} \end{aligned} \tag{5}$$

Excess free-electron (and ion) densities are caused therefore by elevated N-atom concentrations which themselves result from finite N-recombination rates. Thus the unexpected result, suggested earlier in Ref. [9], that ionizational nonequilibrium is due to finite-rate neutral chemistry.

3.2. Mechanism of Gupta, Yos, Thompson, and Lee (GYTL):

The GYTL model[2] differs from the Dunn and Kang model only in the rates for dissociative electron recombination, $NO^+ + e \Leftrightarrow N + O$, and for three-body thermal association, $N + O + M \Leftrightarrow NO + M$. The most significant difference is for the latter reaction as the catalytic efficiencies recommended by GYTL for N, O and NO as third-bodies are 10 times greater than those of Dunn and Kang. This ten-fold increase significantly enhances N-recombination via reactions (5,9,13) in Table 1. When these third-body efficiencies are increased by 10 in Dunn and Kang's model, all computed concentrations are within 30% of those obtained with GYTL. The degree of nonequilibrium for electron populations is smaller with GYTL than with Dunn and Kang (Fig. 3), but the mechanism leading to ionizational nonequilibrium is identical. The excess free-electron population is due to finite N-atom recombination rates, and Eqns. (2-5) apply.

3.3. Mechanism of Park:

Between 4000 and 10000 K, the rate coefficients proposed by Park[3,4] are up to 140 times greater than those of Dunn and Kang, except for reactions (2, 7, 8, 15, 20, 23, 27) in which case they are smaller by up to a factor 30. In particular, the rate coefficient of the dominant electron recombination reaction (12) is about one order of magnitude greater than in Dunn and Kang's model. Nevertheless, the mechanism governing ionizational nonequilibrium is the same as with the previous models and Eqns. (2-5) apply again (with the exception of that for O^+).

3.4. Conclusions

This numerical study of air plasma kinetics yields the unexpected result that, as electron recombination occurs primarily via fast two-body dissociative recombination, ionizational nonequilibrium is caused under certain circumstances by slow neutral recombination. This is unlike the case for atomic plasmas wherein ionizational non-equilibrium is caused by finite three-body electron recombination rates. Although this result was illustrated for the special case of a thermal air plasma recombining from 7500 to 4500 K in 0.6 ms, its applicability also extends to non-thermal plasmas, as mentioned earlier, and to other molecular plasmas because dissociative recombination reactions are in general much faster than three-body electron recombination reactions. Similar conclusions can also be drawn for ionizing plasmas wherein ionization is ultimately limited by molecular dissociation. When this result applies, the modeling of plasma kinetics is greatly simplified, with here only two reactions ($2N + M \rightarrow N_2 + M$ and $N + O + M \rightarrow NO + M$) as opposed to about thirty with the complete mechanism.

As shown in the present study, the extent of nonequilibrium predicted by the three mechanisms varies significantly because of differences between N-recombination rates. Since many of these rates are still not well known,[3] we have conducted experimental studies of ionizational nonequilibrium in air plasmas to test and refine the ideas presented above. Results from these experimental studies are presented in Section 4 of this report.

Table 1. State of Dunn and Kang mechanism at t = 0.6 ms, with reactions listed in order of decreasing efficiency.

Reaction	Forward rate, F (mole-cm^{-3}s^{-1})	Reverse rate, R (mole-cm^{-3}s^{-1})	$\log_{10}\lvert F-R\rvert$	$\frac{R-F}{F+R}$
1. $O + N_2 \Leftrightarrow N + NO$	2.261E–02	2.355E–02	–3.03	0.020
2. $O + NO \Leftrightarrow N + O_2$	2.003E–03	2.881E–03	–3.06	0.180
3. $O_2 + O \Leftrightarrow 3O$	2.534E–05	7.987E–04	–3.11	0.939
4. $O_2 + N_2 \Leftrightarrow 2O + N_2$	3.713E–06	1.170E–04	–3.95	0.939
5. $NO + O \Leftrightarrow N + 2O$	1.481E–06	6.712E–05	–4.18	0.957
6. $NO + N_2 \Leftrightarrow N + O + N_2$	1.356E–06	6.147E–05	–4.22	0.957
7. $N + N_2 \Leftrightarrow 3N$	3.650E–07	1.723E–05	–4.77	0.959
8. $2N_2 \Leftrightarrow 2N + N_2$	2.396E–07	1.131E–05	–4.96	0.959
9. $NO + N \Leftrightarrow O + 2N$	2.140E–07	9.700E–06	–5.02	0.957
10. $O_2 + N \Leftrightarrow 2O + N$	1.465E–07	4.617E–06	–5.35	0.939
11. $N_2 + O \Leftrightarrow 2N + O$	5.287E–08	2.496E–06	–5.61	0.959
12. $O + N \Leftrightarrow NO^+ + e$	4.178E–05	4.305E–05	–5.90	0.015
13. $2NO \Leftrightarrow N + O + NO$	2.001E–08	9.071E–07	–6.05	0.957
14. $O_2 + NO \Leftrightarrow 2O + NO$	1.370E–08	4.318E–07	–6.38	0.939
15. $2O_2 \Leftrightarrow 2O + O_2$	7.788E–09	2.455E–07	–6.62	0.939
16. $N_2 + NO \Leftrightarrow 2N + NO$	7.146E–10	3.373E–08	–7.48	0.959
17. $NO + O_2 \Leftrightarrow N + O + O_2$	6.320E–10	2.865E–08	–7.55	0.957
18. $O + NO^+ \Leftrightarrow NO + O^+$	2.715E–08	3.260E–08	–8.26	0.091
19. $NO + N_2 \Leftrightarrow NO^+ + e + N_2$	8.876E-11	4.145E–09	–8.39	0.958
20. $O + e \Leftrightarrow O^+ + 2e$	4.434E–11	2.487E–09	–8.61	0.965
21. $N_2 + O_2 \Leftrightarrow 2N + O_2$	4.513E–11	2.130E–09	–8.68	0.959
22. $N + NO^+ \Leftrightarrow NO + N^+$	6.979E–08	7.092E–08	–8.95	0.008
23. $2N \Leftrightarrow N_2^+ + e$	6.861E–08	6.938E–08	–9.12	0.006
24. $N_2 + O^+ \Leftrightarrow O + N_2^+$	5.093E–09	4.334E–09	–9.12	–0.080
25. $N + N_2^+ \Leftrightarrow N_2 + N^+$	1.125E–07	1.119E–07	–9.19	–0.003
26. $O + NO^+ \Leftrightarrow O_2 + N^+$	5.899E–10	8.621E–10	–9.57	0.187
27. $N + e \Leftrightarrow N^+ + 2e$	2.455E–13	1.165E–11	–10.94	0.959
28. $NO + O_2 \Leftrightarrow NO^+ + e + O_2$	1.655E–13	7.728E–12	–11.12	0.958
29. $O_2 + N_2 \Leftrightarrow NO + NO^+ + e$	8.280E–16	2.800E–14	–13.57	0.943

4. Recombination mechanism of nonequilibrium air plasmas: experimental results.

4.1. Introduction

As discussed in Section 3, electron recombination in atmospheric pressure air plasmas at temperatures between 4,500 and 7,500 K occurs primarily through fast and equilibrated two-body dissociative recombination reactions, mainly:

$$NO^+ + e \Leftrightarrow N + O, \quad (6)$$

and therefore the extent of ionizational nonequilibrium under these conditions is governed by the rates of the (slow) neutral recombination reaction,

$$N + O + M \rightarrow NO + M. \quad (7)$$

and (but to a lesser extent),

$$N + N + M \rightarrow N_2 + M. \quad (8)$$

Thus, the rate of Reaction 7 determines the extent of ionizational nonequilibrium in air plasmas. Yet, very large discrepancies exist in the rate proposed for this reaction by various authors, namely Dunn and Kang,[1] Gupta et al.,[2] and Park.[3,4] The rate proposed by Park is somewhat greater than the rate of Gupta et al., which is itself greater than Dunn and Kang's rate by a factor 10.

To assess the predictions of the three air kinetics mechanisms,[1-4] experiments were conducted with recombining atmospheric pressure air plasmas generated with the 50 kW inductively-coupled radio-frequency plasma torch described in Section 4.2. below. Initially in equilibrium at a temperature of 7,160 K, the plasma was cooled to ~4,900 K within ~400 μs by flowing at velocities approaching 0.5 km/s through water-cooled, brass test-sections mounted on the plasma torch nozzle exit. Through detailed measurements of temperatures, electron number densities, and emission spectra, it was possible to conclude that the rate of Reaction 7 should be faster than the rates proposed by Dunn and Kang and Gupta *et al.*, and at least as fast as the rate proposed by Park.

Additional experiments were conducted with a nitrogen plasma (with argon addition) recombining from 7200 to 4700 K within 250 μs in order to assess the rate of Reaction 8. These experiments evidenced significant departures from ionizational and chemical equilibrium, in qualitative agreement with predictions based on the model of Park.[4] From these experiments, it was concluded that the rate proposed by Park for Reaction 8 should be accurate to within a factor 3.

Finally, experiments were conducted with a ~10% air - 90 % argon plasma (15.6 slpm air, 162 slpm argon, and 2.3 slpm H_2) cooled from 7,900 K to approximately 2,500 K over a time of ~1.3 ms and a distance of 65 cm. These experiments were conducted in order to provide a better assessment of the rate of Reaction 7 (on which the

pure air studies permitted us to place a lower limit), and to extend the range of our previous work to lower temperatures. The small quantity of H_2 was premixed into the gas for purposes of electron number density measurements. Dilution of ~10% air in argon causes the recombination of nitrogen atoms to be about one order of magnitude slower than in the pure air plasma case as the third body efficiency of argon in Reaction 7 is approximately 20 times smaller than the third body efficiencies of N and O atoms. By slowing the overall N atom recombination, it was possible to observe significant chemical and ionizational nonequilibrium, and thus to place an upper limit on the rate of Reaction 7. Even at this relatively high dilution level, the electron recombination path remains the same as in pure air because electrons still recombine preferentially via the dissociative recombination reaction $NO^+ + e \rightarrow N + O$, even though NO^+ is no longer the dominant ion here. Results from this study indicate that the rate of reaction 7 may be a factor 10 faster than the rate proposed by Park.

In the following sections, we describe first the experimental and diagnostic facility in which the recombination measurements were made. The experimental results and conclusions from recombining air, nitrogen/argon, and air argon plasmas are presented ,and the predictions of the various reaction mechanisms are assessed in light of these results.

4.2. Experimental Facility

A 50 kW TAFA model 66 radio-frequency inductively-coupled plasma torch, powered by a LEPEL model T-50-3 power supply operating at a frequency of 4 MHz, was used to generate air, nitrogen/argon, and air/argon plasmas at atmospheric pressure. The plasmas produced in the torch exit through a 1 cm diameter copper nozzle at velocities up to 1 km/s, and then flow through a water-cooled, 1 cm diameter brass test-section mounted on the exit nozzle of the torch as shown in Fig. 4. The test-section consists of two brass tubes separated by a 3 mm thick annular water cooling passage. Within the test-section, the plasmas are forced to recombine in a well-controlled environment over a predetermined residence time. Several test-sections with lengths between 10 and 65 cm in 5 cm increments were used to vary plasma residence times between approximately 150 μs and 1.3 ms depending on the plasma composition.

Table 2. Summary of experimental conditions. Flow rates in standard liters per minute (slpm).

Plasma	$\dot{m}_{Air}$	$\dot{m}_{N2}$	$\dot{m}_{Ar}$	$\dot{m}_{H2}$	Test-section length, cm
Air	95			1.7	0,15,20,25
N_2/Ar		50	100	1.7	0,10,15
Air/Ar	15.6		162	1.7	0,10,15,40,50,65

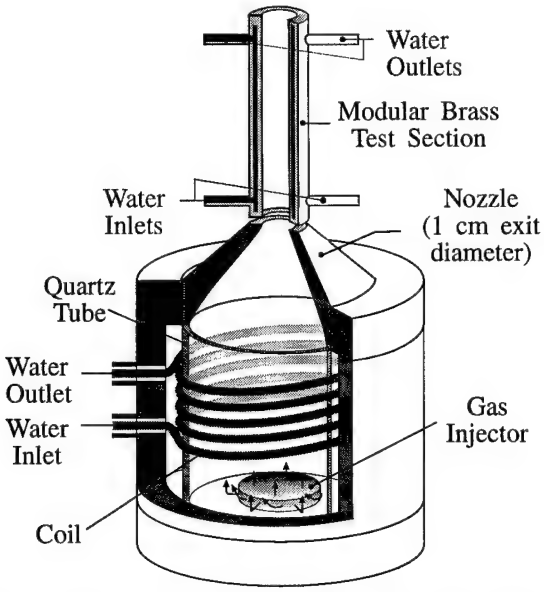

Figure 4. Schematic cross-section of torch head with test-section.

Measurements of temperatures, electron densities, and species concentrations were conducted by means of optical emission spectroscopy at locations ~5 mm downstream of the exit plane of the nozzle (no test-section) and of various test-sections. The measurements were made using a SPEX model 750M, 3/4 meter, scanning monochromator fitted with a Hamamatsu model R1104 photomultiplier tube (see Fig. 5). Two 1200 lines/mm gratings blazed at 200 and 500 nm were used to cover the spectral range of the present study. Absolute intensity calibrations were obtained with two NIST traceable radiance standards: an Optronics model OL550 standard for wavelengths between 300 and 800 nm and a 1 kW Argon Mini-Arc from Arc Applications Research between 200 and 400 nm. A summary of measurement locations and gas flow rates for the three types of plasmas can be found in Table 2.

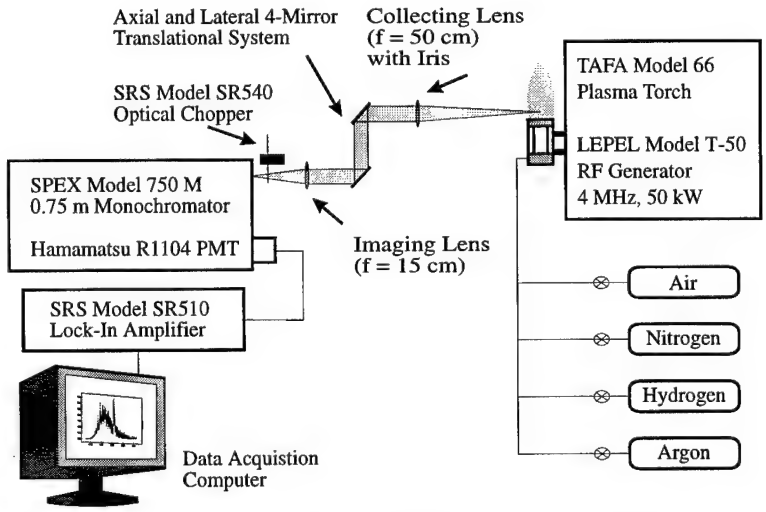

Figure 5. Set-up for emission measurements.

4.3. Recombining Air Plasma

An air plasma flow, initially in equilibrium at a temperature of 7,160 K at the nozzle exit, was cooled to ~4,900 K within ~400 μs over a distance of 25 cm. Temperature, electron density, and spectral emission measurements were made at the exit of the nozzle (0 cm) and of the 15, 20 and 25 cm test-sections. The radial temperature profiles, shown in Fig. 6, were obtained by Abel-inverting lateral profiles of the absolute intensity of the atomic oxygen triplet at 777.4 nm. Electron number densities were measured from the Stark broadening of the H_β line at 486.2 nm (to this end, a small quantity (1.7 slpm) of molecular hydrogen was premixed with 95 slpm of air before injection into the torch). Since electron concentrations are a maximum at the center of the plasma and drop rapidly with radial distance, the electron densities measured from line-of-sight H_β profiles should be very close to centerline values. The lineshapes were corrected for instrumental, Doppler and collisional broadening as in an earlier study.[10] At each location investigated, the electron concentration was found to be close to the equilibrium concentration at the measured temperature (Fig. 7).

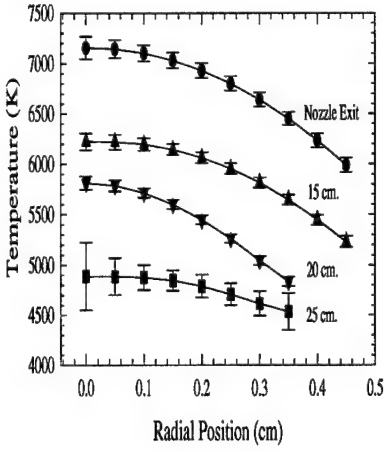

Figure 6. Temperature profiles of the air plasma at 0, 15, 20, 25 cm downstream of the nozzle exit.

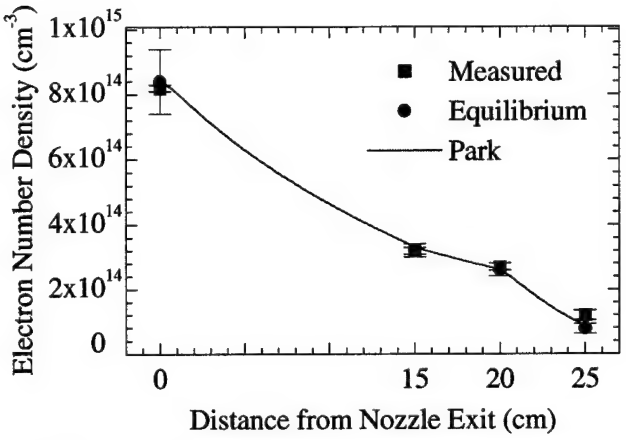

Figure 7. Electron number densities in the air plasma at 0, 15, 20, and 25 cm downstream of the nozzle exit.

Line-of-sight emission spectra were measured at 0, 15, and 20 cm and compared with equilibrium simulations performed with the radiation code NEQAIR2[10-12] using the O-line temperature profiles. Differences between the measurements and the LTE simulations would be indicative of nonequilibrium conditions in the experiment. For instance, as a result of inverse predissociation effects, an overpopulation of N atoms would enhance the radiation emitted by the $C^2\Pi$ state of NO (Ref. [12]), and by the $B^3\Pi$ (Rayleigh-Lewis afterglow[13]) and $C^3\Pi$ (Ref. [3]) states of N_2. An overpopulation of N_2^+ would result in a corresponding increase of N_2^+ (B-X) radiation since, according to the

collisional-radiative model of Park,[14] the N_2^+ B state tends to remain in Boltzmann equilibrium with the ground state. At the three locations investigated, the equilibrium radiation calculations reproduced all measured spectral features originating from the B state of N_2^+, the B state of N_2, the A, B, and C states of NO, and the B state of O_2 within better than 25% (see Fig. 8 for the 15 and 20 cm cases). The present measurements are therefore consistent with at least approximate LTE.

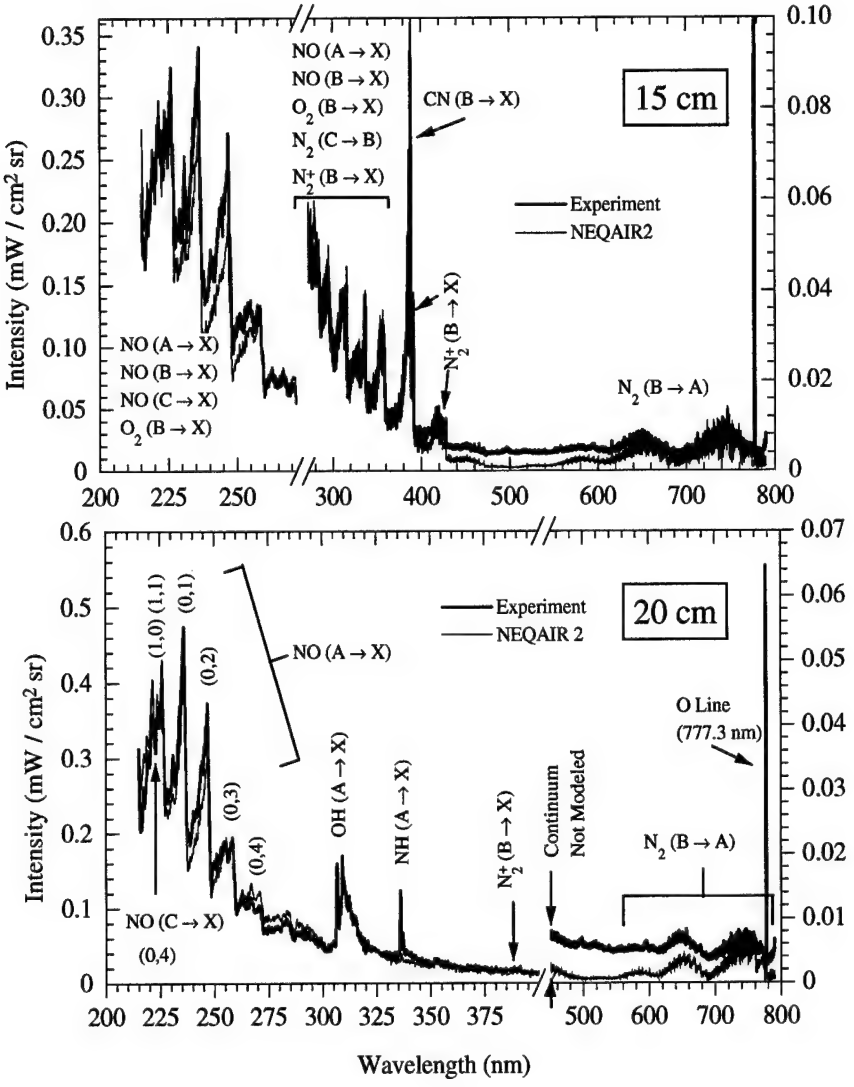

Figure 8. Measured and computed LTE emission spectra of the air plasma at 15 and 20 cm.

These experimental observations were used to assess the reaction mechanisms proposed by Dunn and Kang,[1] Gupta et al.,[2] and Park.[4] To this end, the dynamic evolution of species concentrations along the axis of the plasma flow was modeled as described in Section 3 using the chemical kinetics solver CHEMKIN[5] and the three sets of ~30 reactions and rates.[1,2,4] Diffusion effects were neglected. To calculate centerline

velocities, the velocity and temperature profiles were assumed to be self-similar as the Prandtl number was calculated to be near unity. The velocity profiles were then scaled to match the 1.98 g/s mass flow rate of air/H_2.

Figure 9 shows the predicted nonequilibrium concentration factors, ρ, defined as the ratio of predicted to equilibrium mole fractions.

$$\rho \equiv \frac{x}{x^*(T)}. \tag{9}$$

Thus a value of unity indicates equilibrium, and a value greater than 1 indicates an overpopulation of the given species. Figure 9 also illustrates the discrepancies between the controlling rates of ionizational nonequilibrium, and the resulting uncertainty in the predicted electron concentrations. As can be seen in Fig. 9, the mechanism of Park predicts that the air plasma remains close to equilibrium throughout the reaction zone, in agreement with our experimental observations. In contrast, the mechanisms of Dunn and Kang, and Gupta et al. predict departures from equilibrium in the electron number density by up to a factor 3 at the exit of the 25 cm test-section. Since overall plasma recombination, and in particular electron recombination, is mainly controlled by the rate of Reaction 7 under these conditions, it appears that the rate of Reaction 7 should be at least as fast as the rate proposed by Park.[4]

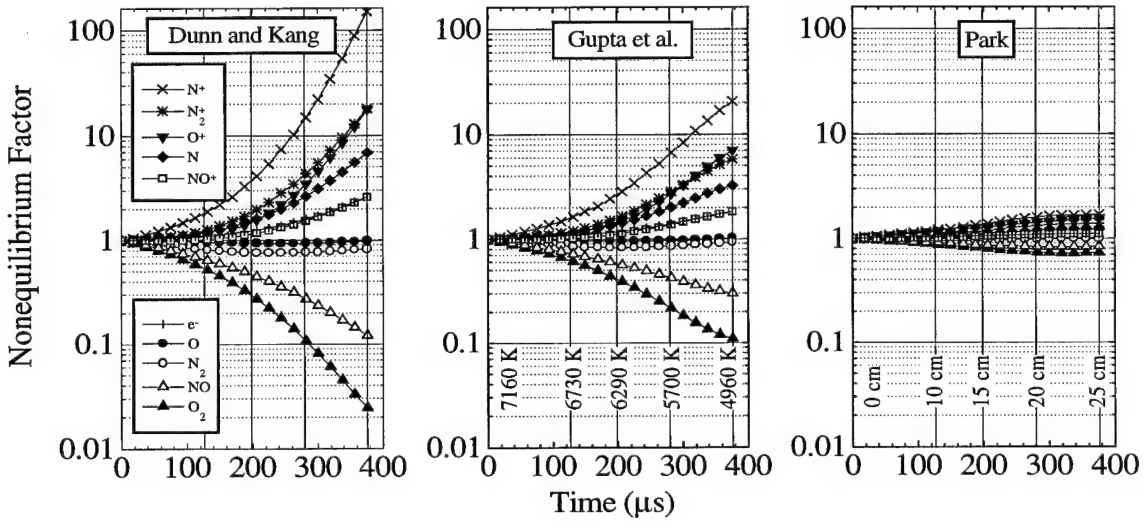

Figure 9. Nonequilibrium factors predicted by three reaction mechanisms for the recombining air plasma.

4.4. Recombining nitrogen plasma

To assess the rate of $N + N + M \Leftrightarrow N_2 + M$ (Reaction 8), separate experiments were conducted with a nitrogen plasma (~100 slpm N_2), premixed before injection into the torch with ~50 slpm of argon to provide stable operating conditions, and ~1.7 slpm of H_2 for electron density measurements. The plasma recombined over 15 cm and ~250 μs from ~7200 to ~4700 K. Measurements were made at the 0, 10 and 15 cm locations. The recombination of N atoms in this nitrogen/argon plasma is slower than in the pure air plasma because the rate of Reaction 8 is from 100 to 10 times slower than the rate of Reaction 7 for temperatures between 4000 and 8000 K. Therefore, it was expected that departures from equilibrium would be larger than in the pure air plasma case.

Temperature profiles at 0 and 10 cm were obtained from the Abel-inverted intensities of lines of argon (763.5 nm) and of hydrogen (H_α and H_β). At both locations, the three temperatures agreed within better than 200 K, thus supporting the assumption of LTE at these locations. Furthermore, spectral simulations based on these temperature profiles and assuming LTE were found to be in excellent agreement with spectral measurements at both locations (see Fig. 10). It was thus concluded that the plasma remained close to LTE from 0 to 10 cm.

At 15 cm however the atomic line intensities were too weak to provide a temperature determination. Instead, the temperature at 15 cm was determined from the absolute intensity of the N_2^+ B-X (0,0) transition band head at 391 nm, using a special procedure to account for possible departures from equilibrium in the population of the emitting B state of N_2^+. This procedure relied on the premise, supported by computations made with the collisional-radiative model of Park[15] for the conditions of this experiment, that the population of the B state stays in Boltzmann equilibrium with the population of the ground state of N_2^+. The population of the ground state of N_2^+ was then determined by an iterative procedure: First, the temperature was determined at 15 cm from the N_2^+ band head intensity assuming N_2^+ to be chemical equilibrium at that location. Based on this temperature, CHEMKIN simulations were made to determine the dynamic evolution of species concentrations from 0 to 15 cm. (For these simulations we used the rates given by Park[3,4] for nitrogen chemistry and the rates of Table 3 for reactions involving argon and hydrogen.) After the first iteration, CHEMKIN predicted an overpopulation of N_2^+ by a factor ~5. Taking into account this overpopulation factor, the temperature at 15 cm was again determined from the N_2^+ band head intensity measurements. This iterative procedure converged to an N_2^+ overpopulation factor of 10 and a centerline temperature of 4720 K (vs. 5200 K at the first iteration).

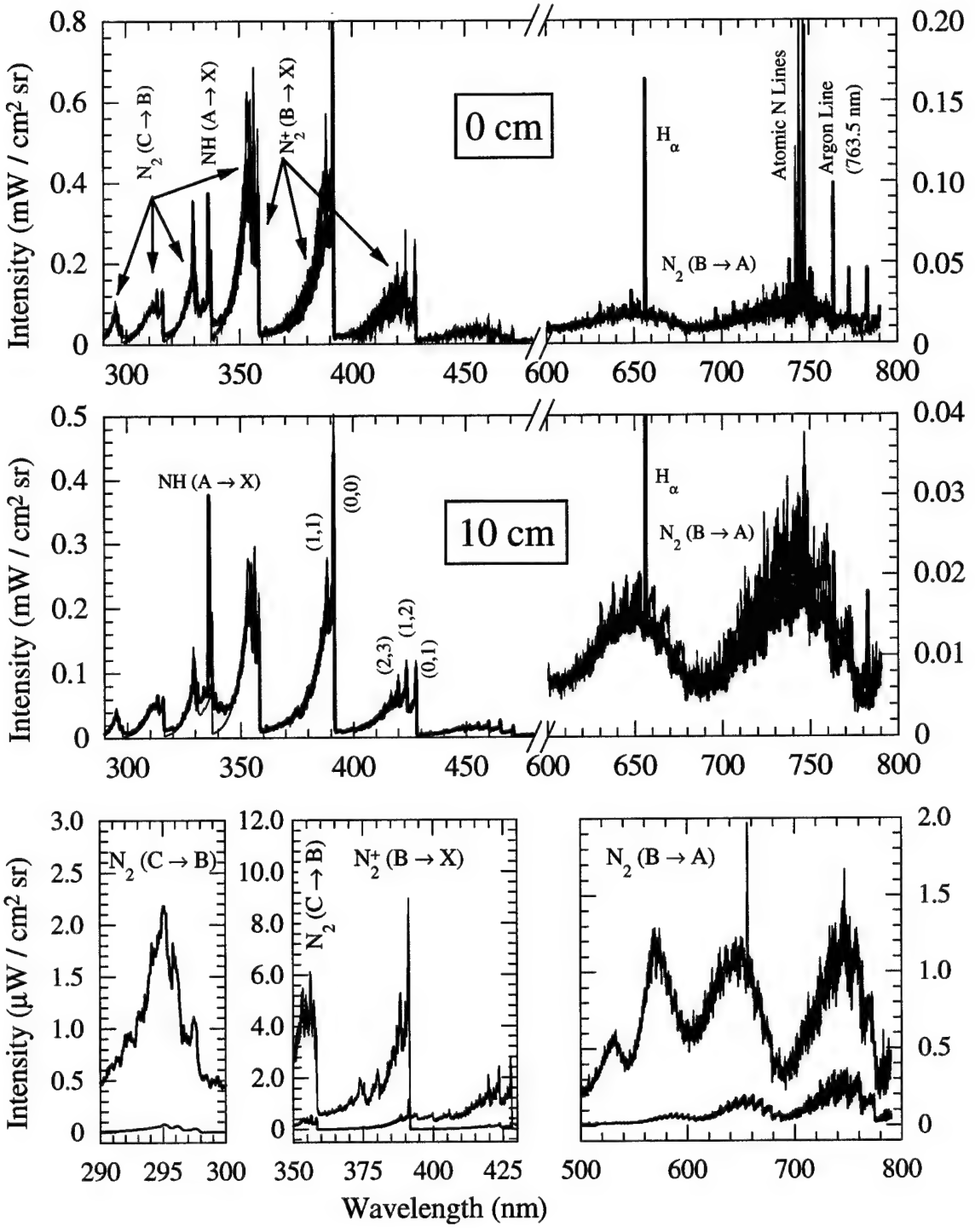

Figure 10. Nitrogen/argon plasma at 15 cm downstream of nozzle exit: Measured spectrum (black) and computed LTE spectrum (black).

Table 3. Forward Rate Coefficients in Arrhenius Form: $A\,T^{n}\exp(-E/T)$

Reaction	A (cm^3/mol s)	n	E (K)	Note
$N_2 + Ar \Leftrightarrow N + N + Ar$	3×10^{21}	–1.6	113,200	From Ref. [16]
$Ar^+ + N_2 \Leftrightarrow Ar + N_2^+$	9×10^{11}	0.6	2,260	(a)
$H + e \Leftrightarrow H^+ + e + e$	1.51×10^{31}	–3.0	158,000	From Ref. [18]
$Ar + e \Leftrightarrow Ar^+ + e + e$	8.26×10^{19}	0.5	135,500	Fit of rate given in Ref. [19]
$H^+ + N \Leftrightarrow H + N^+$	2×10^{13}	0.5	0	(b)

(a) Average of the rates for Ar^+ ($^2P_{1/2}$) and ($^2P_{3/2}$) given in Ref. [20].

(b) Taken identical to the rate given in Ref. [21] for $H^+ + O \Leftrightarrow H + O^+$.

The predicted nonequilibrium factors for major species are shown on Fig. 11. The mechanism predicts that electrons recombine primarily via the fast, equilibrated dissociative recombination reaction $N_2^+ + e \Leftrightarrow N + N$, even though N_2^+ is not the dominant ion. (In fact, the dominant ion is N^+ and the mole fractions of Ar^+ and H^+ are approximately equal to the mole fraction of N_2^+, but the recombination reactions of N^+, Ar^+, and H^+ are ternary reactions, hence significantly slower than the two-body dissociative recombination of N_2^+.) The degree of ionizational nonequilibrium depends mainly on the rates of the (slow) reactions $2N + M \Leftrightarrow N + M$ ($M = N, N_2$). These rates are not necessarily reliable for temperatures below 7000 K because they were extrapolated[16] from measurements above 8000 K for $M = N$ and above 7000 K for $M = N_2$.

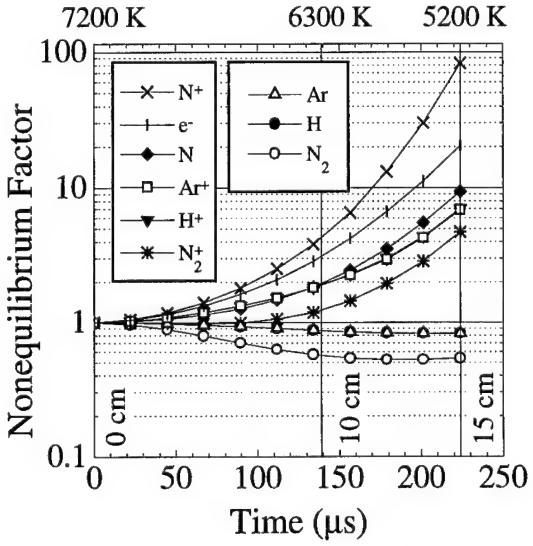

Figure 11. Predicted nonequilibrium factors for the recombining nitrogen/argon plasma.

Electron number densities were also measured at 0, 10 and 15 cm. Fig. 12 shows the comparison between the measured, equilibrium, and predicted electron densities. As can be seen in the figure, electron number densities at 0 and 10 cm were found to be close

to equilibrium. In contrast, at 15 cm an electron overpopulation factor of 135±60 was observed, consistent with (although higher than) the value of 45 predicted with Park's mechanism (see Fig. 11). This overpopulation factor is of course sensitive to uncertainties on the measured temperature since it is defined as the ratio between the measured electron number density and its equilibrium value at the measured temperature. Here, however, the uncertainty on the measured temperature affects the overpopulation factor by less than a factor 2.

Therefore, since here electron recombination is controlled by the rate of Reaction 8, we concluded that the rate proposed by Park for that reaction is accurate to within approximately a factor three over the considered temperature range. Further work is in progress[17] to develop a quantitative coupled flow-chemistry model that could be used to provide a more definite assessment and, if necessary, a corrected value for this rate.

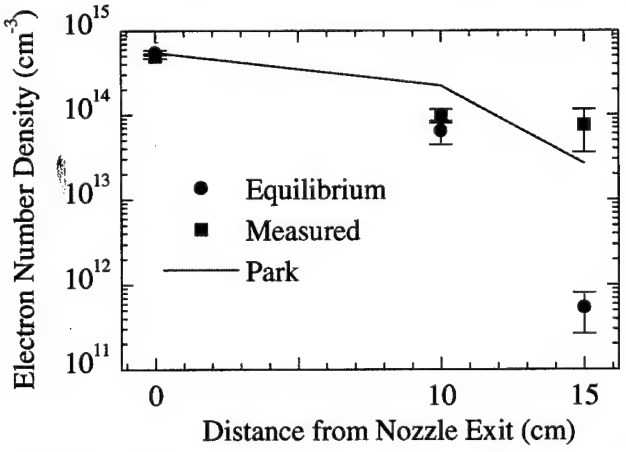

Figure 12. Electron number densities in the nitrogen/ argon plasma.

Experimental confirmation of the slow recombination of N atoms was obtained from spectral emission measurements at 15 cm where the excess free electrons appears conjointly with a significant enhancement of the populations of the B and C states of N_2. This can be seen in Fig. 10 wherein the measured spectrum appears much more intense than the computed equilibrium spectrum, unlike the cases at 0 and 10 cm where the two spectra agree to within better than 10%. To reproduce the experimental spectrum, as shown in Fig. 13, the intensities of the vibrational bands of the N_2 C state had to be uniformly multiplied by a factor ~32, and the intensities of the vibrational bands of the N_2 B state had to be multiplied by the overpopulation factors shown in Fig. 14. The observed overpopulation factor of the C state of N_2, equal to 32, is very different from the predicted nonequilibrium factor of 0.55 (see Fig. 11) for the N_2 molecule. However, the C state being partially predissociative, its population is partially coupled to the population of N atoms. In the case of complete coupling,[22] the overpopulation factor would be equal to the square of the N atom overpopulation which is predicted to be $(\rho_N)^2 \sim 400$ (see Fig. 11). The observed overpopulation of the N_2 C state is therefore qualitatively consistent

with an overpopulation of N atoms. Also indicative of an N atom overpopulation is the large departure from a Boltzmann distribution for the vibrational levels of the B state of N_2 (see Fig. 12). This distribution is characteristic of the Lewis-Rayleigh afterglow mechanism[13] by which N atoms recombine preferentially into levels 10-12 of the B state of N_2 and thus produce the observed vibrational distribution when an excess of N atoms exists. The overpopulation factors observed for these levels thus confirm the presence of an overpopulation of N atoms. A detailed collisional-radiative model is currently being developed for the B and C states of N_2 in order to quantify the N atom overpopulation. It should also be noted that the foregoing observations clearly show that under nonequilibrium conditions great care must be exercised when interpreting both temperatures and concentration measurements.

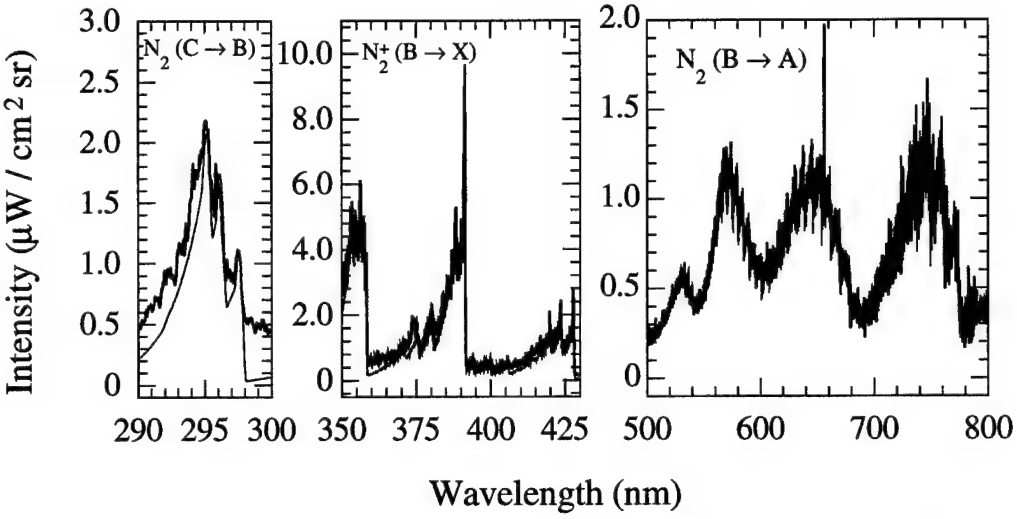

Figure 13. Nitrogen/argon plasma at 15 cm downstream of nozzle exit: Measured spectrum (black) and computed spectrum (red) taking into account nonequilibrium factors of 32 for the C state of N_2, 10 for the B state of N_2^+, and the vibrational-level dependent factors shown in Fig. 14 for the B state of N_2.

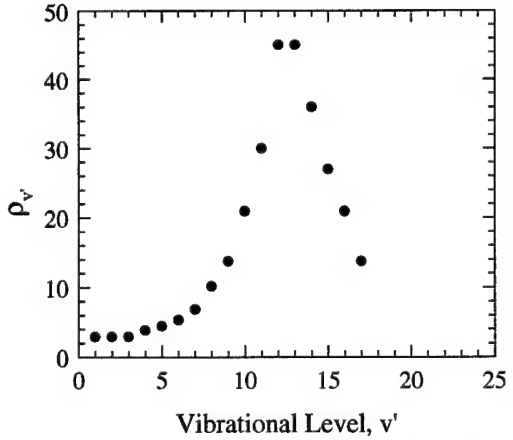

Figure 14. Measured vibrational overpopulation of the N_2 B state (nitrogen/argon plasma).

4.5. Recombining air/argon plasma

In this section, the results of our experimental studies with an air/argon plasma are presented. For these measurements, optical emission was collected at the exit of test sections ranging from 0 cm (nozzle exit) to 65 cm in length. As the temperature varies from ~8000 K at the nozzle exit to ~2500 K at the 65 cm test section exit, several different techniques were developed to obtain temperatures and electron number densities at these locations.

0, 10, and 15 cm.

At these locations, the plasma temperature was sufficiently high to obtain temperature profiles from the Abel-inverted line intensities of oxygen (777.3 nm), argon (763.5 nm) and hydrogen (H_α). At each location, the temperatures determined from the three atomic lines were found to agree within 150 K. The temperature profiles measured at 0, 10 and 15 cm are shown in Fig. 15.

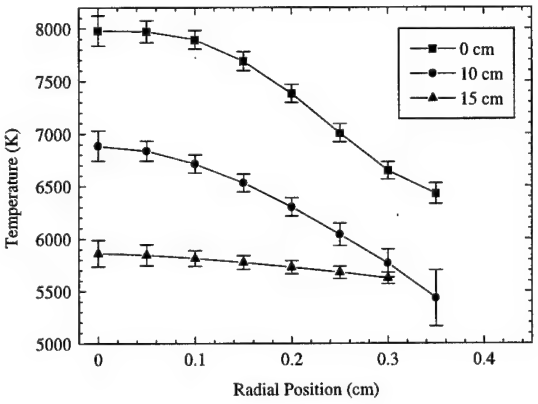

Figure 15. Temperature profiles of the air/argon plasma at 0, 10, and 15 cm downstream of the nozzle exit.

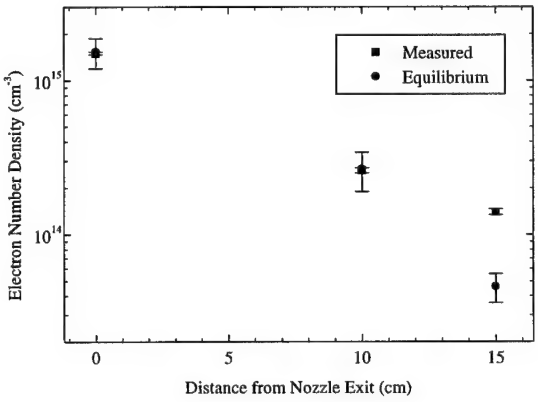

Figure 16. Equilibrium and measured electron number densities (air/argon plasma).

The centerline temperature at these locations is also sufficiently high that a spectrally resolved measurement of the H_β line shape, and thereby of the electron number density,[10] can be obtained. The measured electron number densities match the LTE number densities (Fig. 16) based on the measured centerline temperatures at 0 and 10 cm. At 15 cm, an electron overpopulation of ~3 is measured.

Figure 17 shows comparisons between the equilibrium line-of-sight spectral simulations based on measured temperature profiles and the measured line-of-sight emission spectra. The high centerline temperatures at these locations necessitate consideration of the small but noticeable contribution of the electron recombination continuum to the measured spectra. Due to the uncertainties of accurately calculating this continuum over the measured temperature and wavelength regimes, the continuum is

modeled with a constant value added to the NEQAIR2 simulations such that the computations and measurements match at 360 nm. These small additive constants are 10, 0.7, and 0.1 $\mu W/cm^2/sr$ at the 0, 10, and 15 cm locations, respectively. As discussed in Appendix A, these values are consistent with estimates of the argon recombination continuum.

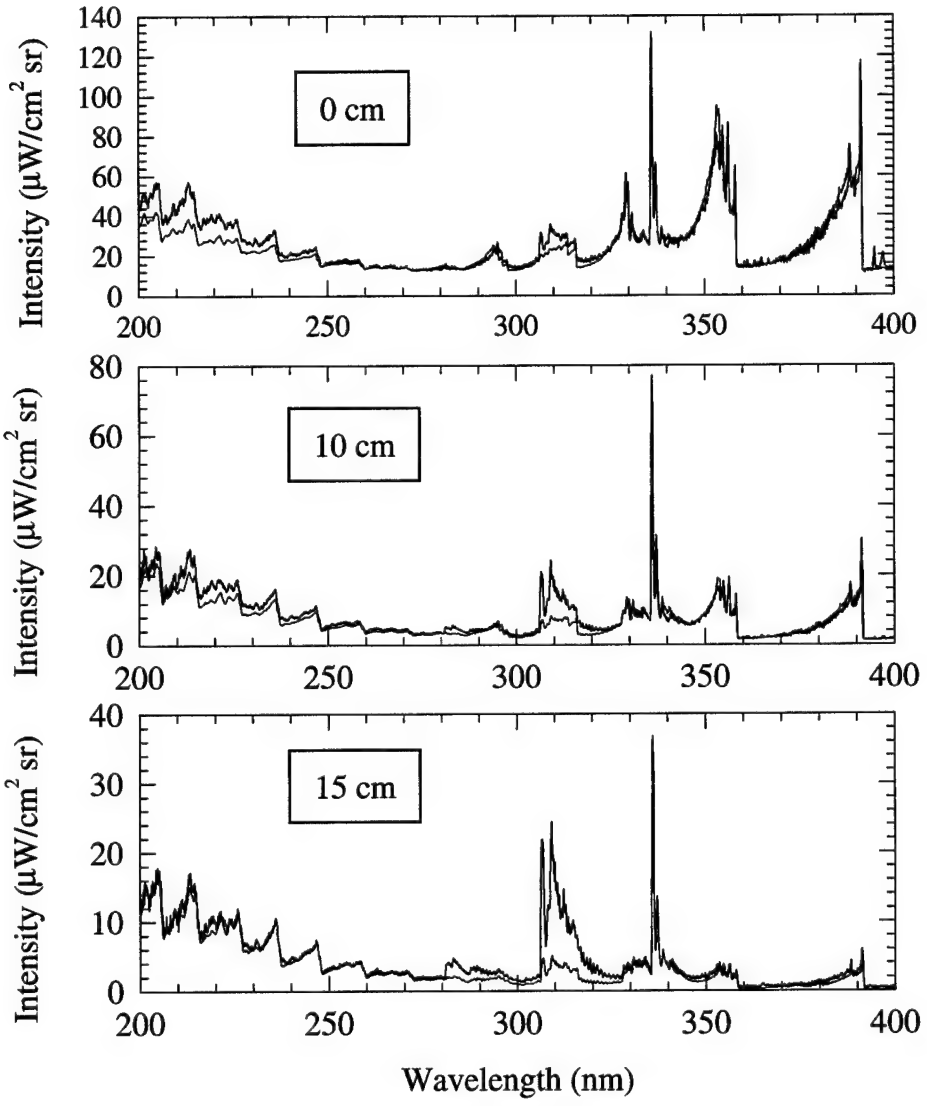

Figure 17. Measured and computed LTE emission spectra of the air/argon plasma at 0, 10 and 15 cm.

As can be seen in Fig. 17, the line-of-sight emission spectra at 0, 10, and 15 cm are reproduced within the 20% experimental uncertainty by equilibrium spectral simulations at the measured temperatures at almost all wavelengths. At 0 cm, the disparity between the two curves near 200 nm is attributed to the inaccuracy in the assumption of a constant electron recombination continuum. Both the argon continuum

model and the empirically determined additive constants show a strong dependence on electron number density and a weaker dependence on temperature. As the electron number density and temperature decrease with distance from the nozzle exit, the magnitude of the continuum becomes negligible in comparison with molecular radiation.

At all three locations, the absolute intensity of the OH A $^2\Sigma^+ \rightarrow$ X $^2\Pi_i$ band ($280<\lambda<315$ nm) is not well reproduced by the spectral simulations. This discrepancy can be explained by considering the LTE number density of the OH A state (Fig. 18) which has a maximum at approximately 3700 K, well below all temperatures at a radius of 0.35 cm. The discrepancy therefore arises as the measured OH emission at the 0, 10, and 15 cm locations originates in the outer edges ($r > 0.4$ cm) of the plasma where the Abel-inverted atomic line intensities are too weak to provide reliable temperature information for the spectral simulations.

In summary, at 0 and 10 cm all measurements are consistent with LTE. At 15 cm, the spectral emission is also consistent with LTE despite the small measured electron overpopulation.

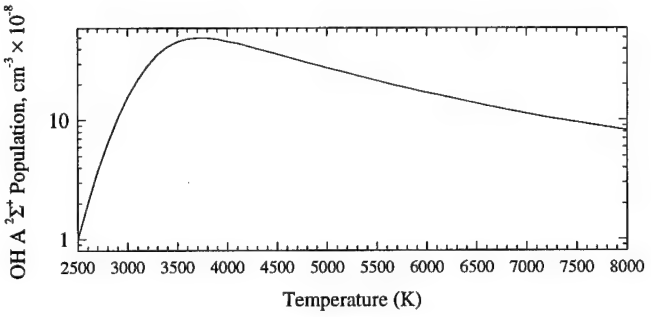

Figure 18. LTE OH A state concentration for the air/argon plasma.

40, 50, 65 cm

At these locations, the excited state populations of atomic species are so small that atomic lines cannot be seen in emission. However, the temperatures can still be accurately deduced by examining the temperature sensitive shape of the measured OH $A^2\Sigma^+ \rightarrow X^2\Pi_i$ band. In particular, the relative strengths of the two peaks at 306.8 and 309.2 nm strongly depend on rotational temperature as both peaks belong to the (0,0) band. The decrease in intensity beyond 311 nm is sensitive to both vibrational and rotational temperatures. As the centerline temperature for these locations was found to be less than 3700 K, the modeling of the measured line-of-sight OH $A^2\Sigma^+ \rightarrow X^2\Pi$ emission spectra does not encounter the difficulties discussed previously.

The centerline temperature is determined by comparing numerical OH spectra[23] at various temperatures normalized to the 309.2 nm peak to the measured line of sight

spectra. This shape-matching technique yields centerline temperatures with an accuracy of ~200 K. The remainder of the temperature profile is obtained from the Abel-inverted intensity of the 306.8 peak relative to the 304 nm baseline. The measured line-of-sight OH spectrum at 40 cm is compared with the synthetic spectrum in Fig. 19. The agreement between the *absolute* calculated and measured intensities is typical of all locations.

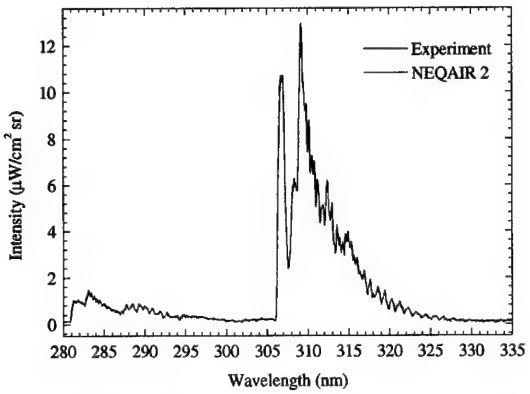

Figure 19. Comparison of measured and calculated line-of-sight OH A→X band at 40 cm (air/argon plasma).

At 50 and 65 cm this procedure must be slightly modified as the plasma was found to be in chemical and ionizational nonequilibrium. The shape of the measured spectra still determines the centerline temperature. However, an overpopulation factor for the OH A state ($\rho_{OH\ A}$) must be determined such that the numerical and measured line-of site spectra agree absolutely. This method, of course, assumes that the overpopulation factor is uniform across the plasma. The OH temperature profiles so determined are displayed in Fig. 20.

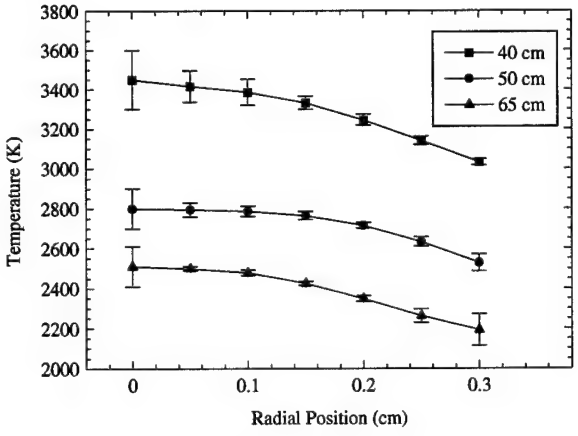

Figure 20. Temperature profiles of the air/argon plasma at 40, 50, and 65 cm downstream of nozzle exit.

Features emanating from the NO A, C, and D states and from the N_2 C state are also visible at these locations. Their shapes are not as sensitive to rotational or vibrational temperature as the OH spectrum but can be used to confirm the deduced temperatures within 500 K. Electronic overpopulation factors are determined in the same manner as for the A state of OH.

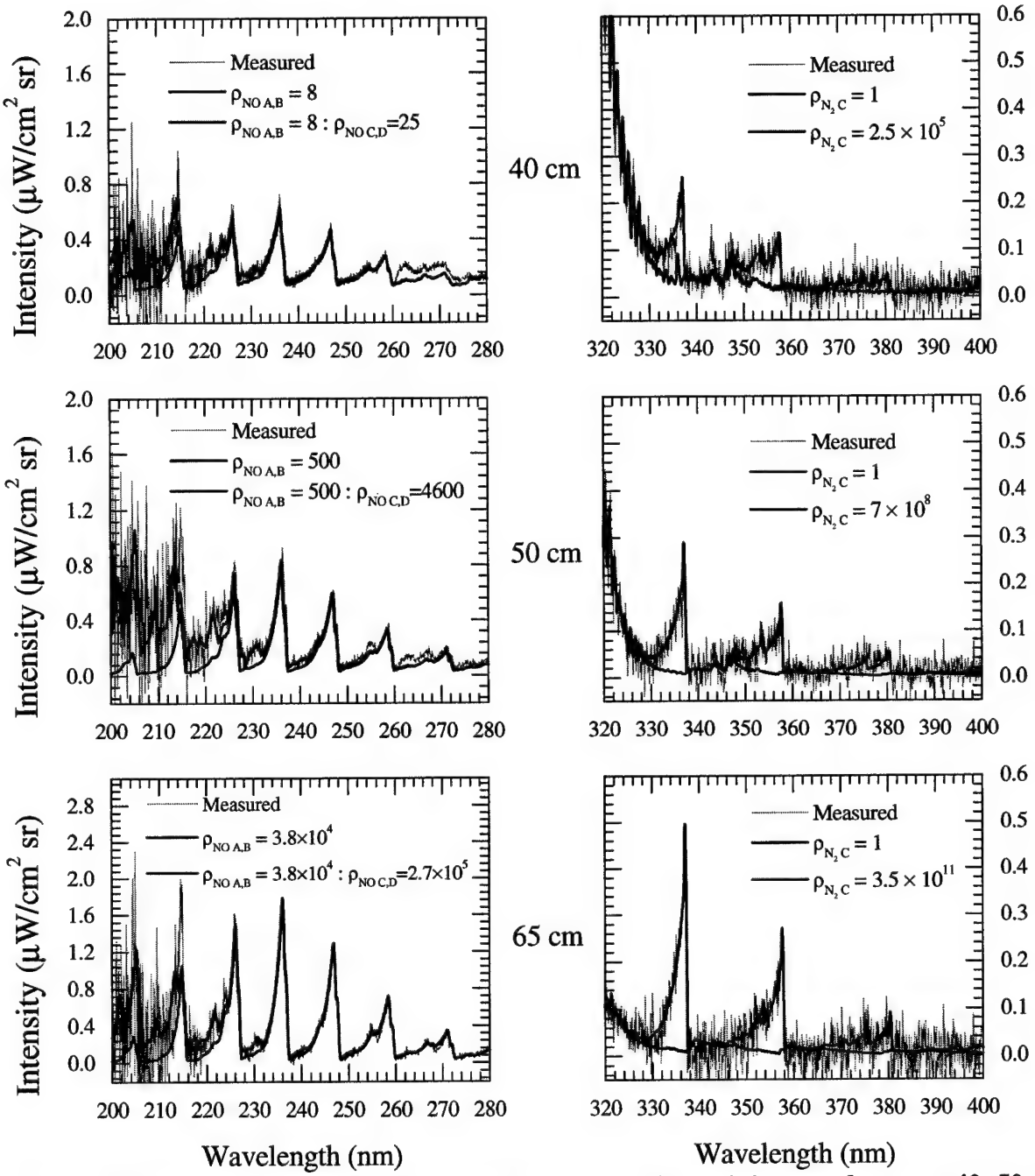

Figure 15. Measured and computed emission spectra of the air/argon plasma at 40, 50, and 65 cm. Included in the spectral simulations are the NO β (B→X), γ (A→X), δ (C→X), ε (D→X), O_2 Schumann-Runge (B→X), N_2 2^+ (C→B), $N_2^+1^-$(B→X), OH (A→X), and NH (A→X) transitions. Unless specified otherwise, the nonequilibrium factors for all species are set equal to 1 in the simulations.

The experimental (gray line) and numerical line-of-sight spectra at the 40, 50 and 65 cm locations are shown in Fig. 21. The region between 280 and 320 nm is excluded as the much more intense OH A-X band (13, 8, and 3 $\mu W/cm^2/sr$ respectively) dwarves the other spectral features. Below 280 nm, the red line in Fig. 21 corresponds to the line-of-sight spectrum obtained by assuming that all electronic levels of NO, except the A and B states, are in LTE at the measured temperature. The NO A state overpopulation, $\rho_{NO\ A}$, is determined by matching the height of the NO γ (0,1) band at 236.2 nm. The blue curve (below 280 nm) accounts for the overpopulation factors of the NO A, C, and D states, with $\rho_{NO\ C}$ determined from the NO δ (0,5) band at 230.8 nm and $\rho_{NO\ D}$ assumed to be equal to $\rho_{NO\ C}$. The NO C and D states are likely to be in equilibrium with each other due to very fast collisional exchange[24,25] owing to the small energy difference between their potential energies. The spectral locations of relevant NO δ and ε transitions are shown in Fig. 22.

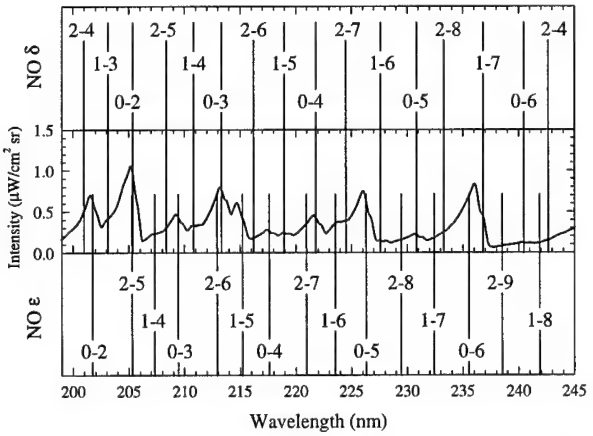

Figure 22. Band origins for NO δ and ε. The spectral emission curve is the non-LTE NEQAIR2 calculation from the 50 cm test section (see Fig. 21).

Above 320 nm, the red curve corresponds to the computed equilibrium spectrum, and the blue curve is obtained by including the measured $\rho_{N_2\ C}$ in the simulation. All measured overpopulation factors are summarized in Table 4.

Table 4. Measured excited state overpopulation factors

Electronic state	Transition name	Term energy (cm^{-1})	ρ 40 cm	ρ 50 cm	ρ 65 cm
NO A	NO γ	43966	8	500	3.8×10^4
NO C	NO δ	52180	25	4600	2.7×10^5
NO D	NO ε	53085	25	4600	2.7×10^5
N_2 C	2+	89137	2.5×10^5	7×10^8	3.5×10^{11}
OH A	A→X	32684	1	4.25	18.3

Kinetic Analysis

The air plasma and nitrogen/argon plasma experiments were used to examine the applicability of the Dunn and Kang,[1] Gupta et al.,[2] and Park[3,4] mechanisms to recombining atmospheric pressure plasmas. As it was concluded that the Park mechanism most adequately described our measurements in pure air,[22,26] only this mechanism will be considered here. The kinetics solver CHEMKIN[5] was used for one-dimensional modeling of the plasma chemistry along the axis of the flow. Rates to describe the relevant hydrogen and argon chemistry, taken from Laux et al.,[22] were appended to the Park mechanism. Rates for O_2[27] and NO[28,29] thermal dissociation by argon were taken from the NIST chemical kinetics database[30] (Table 5). Dissociative and three-body electron attachment reactions such as:

$$O_2 + e \Leftrightarrow O + O^-,$$

$$O_2 + e + e \Leftrightarrow O_2^- + e,$$

while certainly important in low temperature air plasmas,[31] are not considered in the present study because the concentrations of the negative ions are negligible at temperatures above 2000 K. Nor did we consider the N_4^+ dimer formed via the following reaction:[31]

$$N_2 + N_2^+ + M \Leftrightarrow N_4^+ + M,$$

as it is likely to be very unstable in atmospheric pressure gases at temperatures much above room temperature.

Table 5. Forward rate coefficients in Arrhenius form: $A\,T^n \exp(-E/T)$

Reaction	A (cm^3/mol/s)	n	E(K)
$O_2 + Ar \leftrightarrow O + O + Ar$	1.2×10^{14}	0	54280
$NO + Ar \leftrightarrow N + O + Ar$	9.64×10^{14}	0	74697

To calculate centerline velocities, the velocity profiles were assumed to be self-similar to the measured temperature profiles as the Prandtl number was calculated to be near unity. The velocity profiles were then scaled to match the 4.7 g/s mass flow rate of argon/air/hydrogen. The inferred centerline axial velocity was found to decrease from 1060 to 330 m/sec between 0 and 65 cm. The resulting temperature history is displayed in Fig. 23.

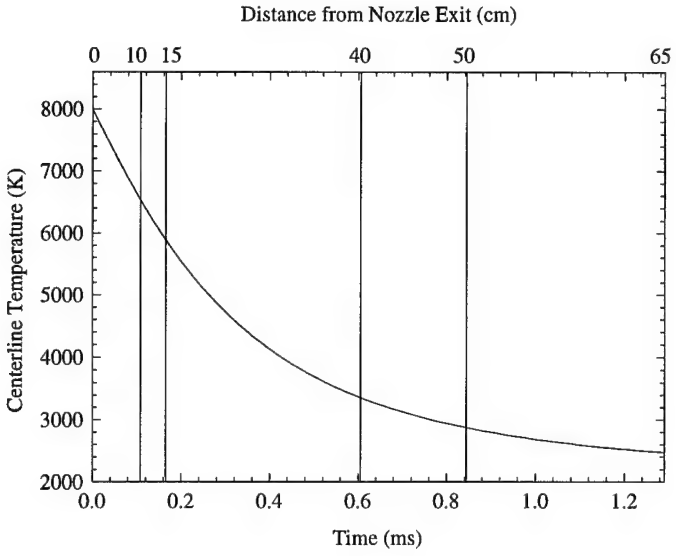

Figure 23. Centerline temperature history based on velocity calculations (air/argon plasma).

To substantiate the velocity predictions, the calculated velocity profiles were used with the measured temperature profiles to calculate the total power in the plasma at each axial location. The calculated decrease in plasma power as a function of distance from the nozzle exit was then compared with calorimetric measurements of the power removed by the water-cooled test sections. Satisfactory agreement is found (Fig. 24).

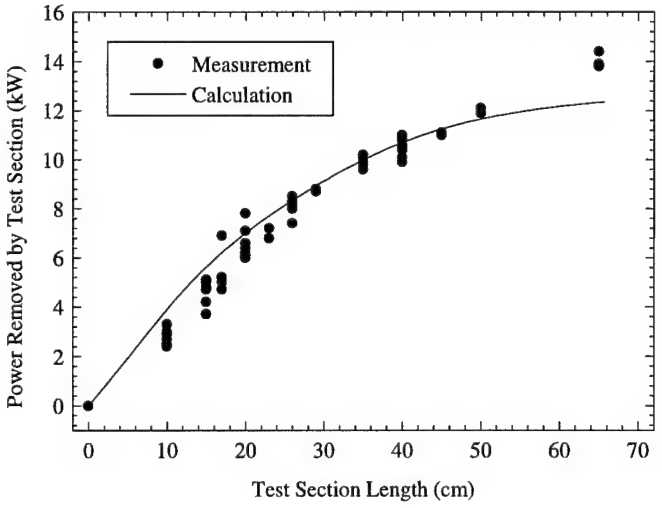

Figure 24. Comparison between measured and calculated power removed by test sections in the air/argon plasma experiments.

The predicted nonequilibrium factors for major species are shown in Fig. 25. The mechanism again predicts that electrons almost exclusively recombine through the fast and equilibrated two body dissociative recombination $NO^+ + e \leftrightarrow N + O$, even though

NO^+ is not the dominant ion. Therefore the three body recombination reactions control the electron overpopulation.

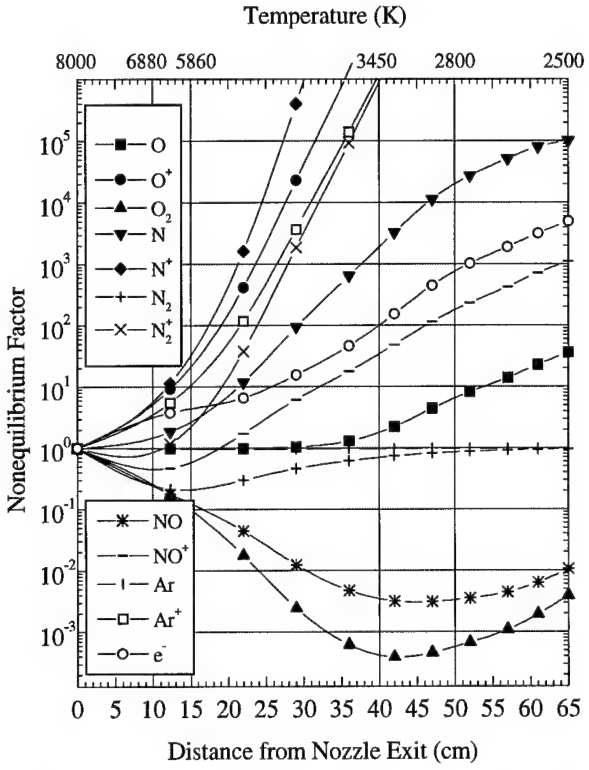

Figure 25. Predicted nonequilibrium factors for the air/argon plasma.

Despite the fact that overpopulation factors have been measured for various molecular *excited* states, situations exist which enable the data to be used to evaluate the accuracy of the chosen *ground state* kinetic mechanism.

The measured NO C state overpopulation, for instance, can be compared with an upper bound value corresponding to the situation where, owing to strong collisional coupling, the C state is in Saha equilibrium with the free electrons. This process corresponds to the following reaction being equilibrated:

$$NO^+ + e + e \leftrightarrow NO\ (C) + e.$$

This equilibrium is described by the Saha relation:

$$\frac{n_{NO^+} n_e}{n_{NO\,C}} = 2\frac{g_{NO^+}}{g_{NO}}\left(\frac{2\pi m_e kT}{h^2}\right)^{3/2} \frac{Z^{vJ}_{NO^+}}{Z^{vJ}_{NO\,C}} e^{-E^{C\lambda}/kT} \qquad (10)$$

where Z^{vJ} represents the rovibrational partition function of the C state of NO or the ground state of NO^+, and $E^{C\lambda}$ is the energy difference between the NO first ionization potential and the C state term energy. The Saha equation can be expressed succinctly as:

$$\rho_{NO\,C} = \rho_{NO^+}\rho_e$$

by dividing each side of Eq. 10 by equilibrium values.

There is another possible mechanism by which the NO C state population can be enhanced. Indeed, the NO C state predissociates and therefore can be populated through inverse predissociation.[12] Given that these rates are fairly large when compared with the rates of C state spontaneous emission and collisional excitation processes,[12] it is reasonable to assume that the reaction

$$NO\,(C) \leftrightarrow N\,(^4S) + O(^3P)$$

is approximately equilibrated. Since this reaction involves ground state N and O atoms, it follows that:

$$\rho_{NO\,C} \cong \rho_N\rho_O\,.$$

It is interesting to note that since Park's mechanism predicts that the dissociative recombination reaction $NO^+ + e \leftrightarrow N + O$ is fast and equilibrated, the following relation holds at all locations:

$$\rho_{NO^+}\rho_e \cong \rho_N\rho_O$$

Thus both Saha coupling and predissociation coupling yield the same predicted upper limit for the overpopulation factor of the NO C state. Numerical predictions for the upper bound on $\rho_{NO\,C}$ are compared with measurements in Fig. 26a. As can be seen in Fig. 26a, the upper bound determined with Park's mechanism appears consistent with the measured overpopulation. However, since it is expected that the coupling due to predissociation/inverse predissociation is very strong for the NO C state, one would expect a closer agreement between the measurements and the predicted upper bound. It would thus appear that ρ_N is too high as ρ_O is relatively close to unity. Furthermore, since the three body recombination of NO accounts for about 38 to 20 % of the total N atom consumption between 15 and 60 cm downstream of the nozzle exit (the balance being due to the Zeldovich reactions whose rates can be considered well known), the rate of $N + O + M \leftrightarrow NO + M$ may be too slow. While Park concludes that this rate is known within a factor three,[3] examination of his compilation of relevant NO thermal dissociation rate measurements seem to warrant a factor ten uncertainty on this rate. Thus, Fig. 26b includes predictions based on calculations in which the third body efficiencies for this reaction, excluding M = Ar, have all been enhanced by a factor ten. (The argon third body efficiency was not enhanced as the rate of thermal dissociation of NO by argon seems to be known well.[30]) It can be seen from Fig. 26 that multiplying the third body efficiencies by a factor 10 improves the agreement between measurements and predictions for test-sections ≤45 cm, but produces a recombination rate that is too fast at

longer distances. Several issues must be examined in order to draw more definite conclusions about these third body efficiencies. First, a detailed collisional-radiative model is warranted to better determine the degree of coupling between the NO C state and electrons or N and O atoms via the two processes previously mentioned. And second, possible departures from a Maxwellian distribution for the free-electrons and their consequences on rate coefficients should be considered. A preliminary analysis of these effects (see Appendix B) indicates that departures from a Maxwellian distribution may occur at locations > 35 cm. These various issues are currently being examined in order to provide a better assessment of the rate of NO thermal dissociation.

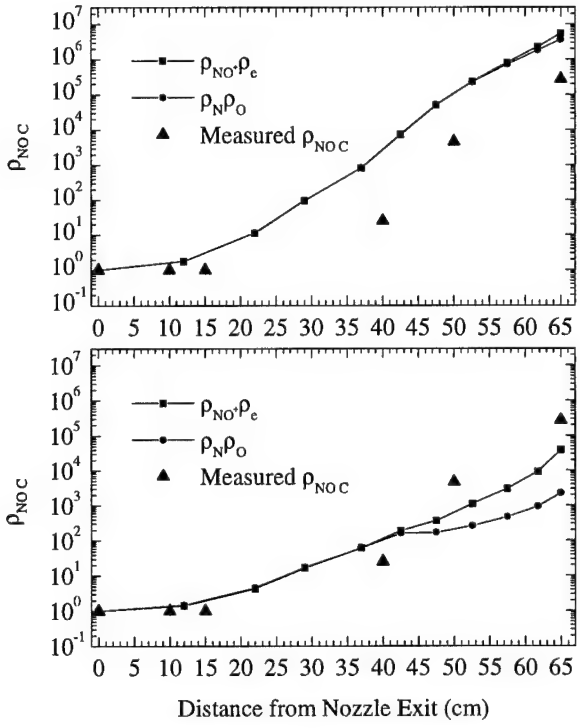

Figure 26. Comparison between calculated and measured NO C state nonequilibrium factors. Top frame (26a) uses Park's mechanism. Bottom frame (26b) uses Park's mechanism with a rate of NO thermal dissociation enhanced by a factor 10.

Similar arguments can be made with regards to the interpretation of the measured N_2 C state overpopulation. If the N_2 C state is in Saha equilibrium with the free electrons, we then have:

$$\rho_{N_2\,C} = \rho_{N_2^+}\rho_e .$$

This equation defines an upper bound for the N_2 C state overpopulation corresponding to full collisional coupling with free electrons. Another upper bound corresponds to equilibrium between the N_2 C state and ground state nitrogen atoms as a result of predissociation and its reverse. This upper bound is defined by:

$$\rho_{N_2 C} = \rho_N^2 .$$

It should be noted that this is the model employed by the NEQAIR collisional radiative model[14] for the N_2 C state. Figure 27a shows the comparison between the measured N_2 C state overpopulation and the upper bounds just described. As can be seen in Fig. 27a, these two upper bounds do not coincide. This is because Park's mechanism predicts that the dissociative recombination of N_2^+ is not equilibrated. As can also be seen in Fig. 27a, the measured N_2 C state overpopulation is larger than the "upper bound" curve corresponding to predissociation coupling. This may indicate that Saha coupling is stronger than predissociation coupling for the C state of N_2. (It should be noted that unlike the NO C state, not all rovibrational levels of the N_2 C state predissociate and therefore predissociation coupling may not be as strong as in the case of NO C.) Nevertheless, the upper bound defined by the Saha coupling appears consistent with the measurements. The effect of increasing the third body efficiencies of N + O + M $\leftrightarrow$ NO + M by 10 is shown in Fig. 27b. As was the case for the NO C state analysis, better agreement is obtained between the Saha coupling curve and the measured N_2 C overpopulation at locations $\leq$ 45 cm. Yet it is clear that a more detailed collisional-radiative model is required to interpret the nonequilibrium data.

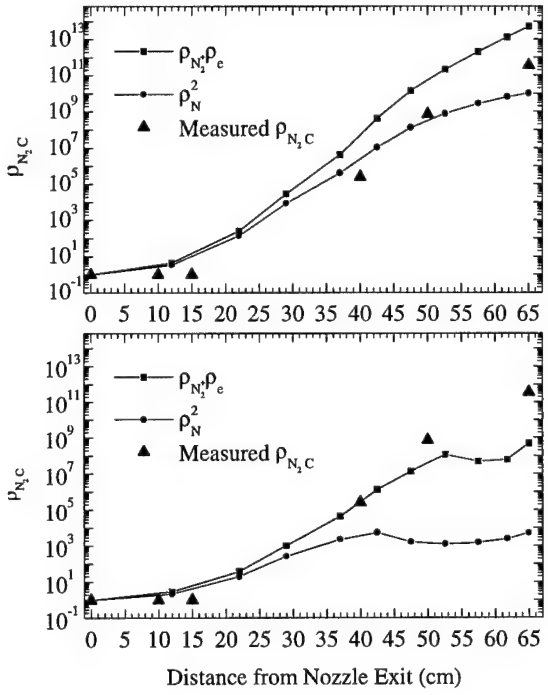

Figure 27. Comparison between calculated and measured N_2 C state nonequilibrium factors. Top frame (27a) uses Park's mechanism. Bottom frame (27b) uses Park's mechanism with rate of NO thermal dissociation enhanced by a factor 10.

Finally the measured electron number densities are compared with those predicted using Park's mechanism. At 0, 10, and 15 cm, direct measurements of n_e were made via the Stark broadening of the H_β line at 486.1 nm. Error bars on these data points (Fig. 28) reflect uncertainties on measured electron number densities and on centerline temperatures. At the exit of longer test-sections, the intensity of the H_β line was very weak, and therefore no direct measurements of electron number densities could be made. However, Park's model predicts that the NO^+ dissociative recombination is equilibrated and that within a factor 3, $\rho_{NO^+} = \rho_e$. It follows that $\rho_{NO\,C}$ should approximately equal $(\rho_e)^2$. Figure 28 compares the predicted electron number densities and those determined from the measured overpopulation factors of the C state of NO. It should be noted that this powerful technique of electron number density determination has never been applied by other researchers prior to the present work. These results support the same conclusions as those drawn from analyzing the NO C and N_2 C state overpopulations, namely that the rate proposed by Park for N+O + M $\Leftrightarrow$ NO + M appears to be to slow by about a factor 10.

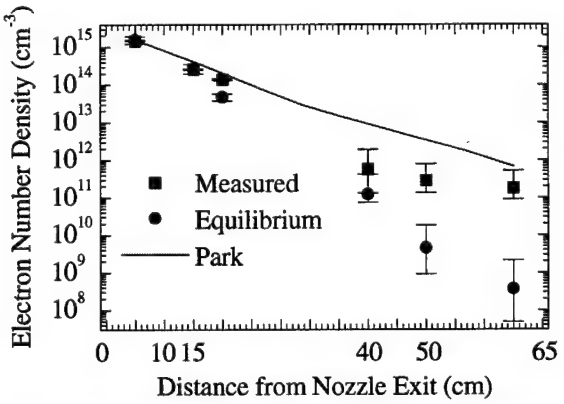

Figure 28. Electron number densities in the air/argon plasma.

4.6. Conclusions

An analysis of the kinetics of recombining air plasmas was presented. This analysis shows that electron recombination occurs primarily through two-body dissociative recombination reactions. As a result, overall electron recombination rates are significantly greater than those for three-body electron recombination, and the extent of ionizational nonequilibrium is governed by the rates of relatively slow three-body atom recombination reactions such as N + O + M $\rightarrow$ NO + M and 2N + M $\rightarrow$ N_2 + M. In order to test the predictions of three reaction mechanisms widely used for air plasma chemistry, experiments were conducted with air, nitrogen, and air/argon plasmas in which various degrees of chemical and ionizational nonequilibrium were produced. In all three cases, measurements of electron number densities and excited electronic state concentrations were made in order to assess the recombination models and the rates of the controlling

three-body neutral recombination reactions. Predictions based on the model proposed by Park were found to be qualitatively consistent with our observations. Before more quantitative conclusions can be drawn, several issues must be addressed. First, a detailed collisional-radiative model must be developed to better assess the degree of collisional coupling between electronic excited states and electrons or atoms. Second, the simple one-dimensional model used to predict the time-temperature history of the recombining plasma should be refined. Third, the consequences on the rates of possible departures from a Maxwellian electron energy distribution must be examined.

Nevertheless, it already appears from the present work that all measurements support the proposed air plasma recombination mechanism. In addition, while the rate of three-body N_2 recombination appears to be accurate within a factor 3, our measurements support a rate of three-body NO recombination that is ~10 times faster than the rate proposed by Park and Gupta et al., and ~100 times faster than the rate of Dunn and Kang. Finally, a new

The results from this work have important implications regarding the transport of air plasmas and the development of methods for creating and sustaining elevated nonequilibrium electron number densities in low temperature, atmospheric pressure air. As discussed in this report, the overall recombination of electrons results from and is controlled by the recombination of neutral species, in particular that of N and O into NO. It is clear therefore that in order to maintain elevated electron number densities, the recombination of NO must be inhibited. Maintaining a high level of NO dissociation may thus be the key to attaining and efficiently sustaining the desired elevated electron number densities in the framework of our newly started Air Plasma Rampart program.

Appendix A. Argon Continuum Radiation

The continuum radiation resulting from electron-ion free-bound (ε_{fb}^{ei}), electron-neutral free-free (ε_{ff}^{en}), and electron-ion free-free (ε_{ff}^{ei}) interactions can in fact be estimated. These three continua correspond to the following processes:

$X^+ + e \leftrightarrow X + h\nu$,

$X + e \leftrightarrow X + e + h\nu$,

$X^+ + e \leftrightarrow X^+ + e + h\nu$,

where X represents Ar, O, N, O_2, N_2, or NO. Argon comprises ninety percent of the plasma in the present experiments and is likely to be the major source of the observed continuum. The argon continuum emission is modeled as follows:[33]

$$\varepsilon = \varepsilon_{fb}^{ei} + \varepsilon_{ff}^{en} + \varepsilon_{ff}^{ei}$$

$$\varepsilon_{fb}^{ei} = C_1 n_e n_i [1 - \exp(-\frac{hc}{\lambda k T_e})] g_i \frac{\xi_{fb}(\lambda, T_e)}{\lambda^2 T_e^{0.5} Z_i}$$

$$\varepsilon_{ff}^{ei} = C_1 n_e n_i \exp(-\frac{hc}{\lambda k T_e}) g_i \frac{\xi_{ff}(\lambda, T_e)}{\lambda^2 T_e^{0.5}}$$

$$\varepsilon_{ff}^{ei} = C_2 n_e n_a \frac{T_e^{1.5} Q(T_e)}{\lambda^2} \left[1 + \left(1 + \frac{hc}{\lambda k T_e} \right)^2 \right] e^{-\frac{hc}{\lambda k T_e}}$$

where $C_1 = 1.631 \times 10^{-43}$ $Wm^4K^{1/2}sr^{-1}$, $C_2 = 1.026 \times 10^{-34}$, n_e, n_a, and n_i are the electron, Ar, and Ar^+ densities, respectively, g_i is the electronic ground state degeneracy of Ar^+, ξ_{fb} the free-bound Biberman factor,[34] Z_i the Ar^+ partition function, ξ_{ff} the free-free Biberman factor, and $Q(T_e)$ the averaged electron-neutral collision cross section. The values of ξ_{fb}, ξ_{ff} and $Q(T_e)$ are specified by Gordon.[35] The results of this model are shown in Fig. A.1 for a 2 mm diameter, uniform temperature, LTE argon plasma. The calculated values of 2.5, 2.4, and 2.2 $\mu W/cm^2/sr$ at 360 nm are consistent with the constants added to the numerical spectrum within a factor 20. Estimates of the contribution from air species to the recombination continuum are difficult to obtain as we are not aware of calculations and measurements for these quantities at temperatures below 9000 K.[36,37]

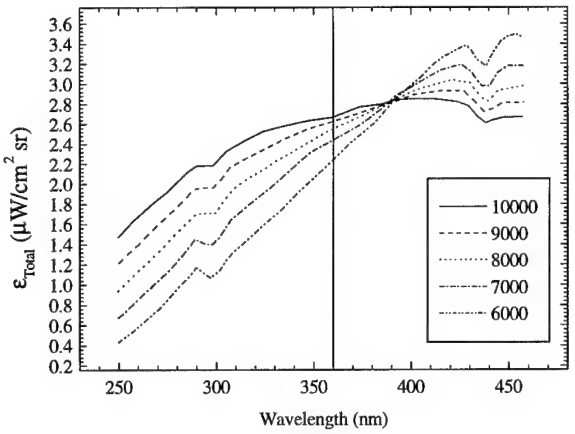

Figure A1. Total radiative recombination emission coefficient for a 1 atm LTE argon plasma. Calculations are for a 2 mm diameter plasma observed through a monochromator with a 0.44 nm instrument broadening.

Appendix B. Electron Energy Distribution

Both the predicted and measured chemical/ionizational nonequilibrium warrant consideration of the validity of applying Park's reaction mechanism to this data analysis. In particular, it is possible that the rates of importance may be dramatically altered by departures from equilibrium in the Maxwellian electron energy distribution upon which Park's rates rest. Sufficient conditions for the existence of a Maxwellian distribution can be obtained by consideration of the first Cartesian-tensor equation formed from the

electron Boltzmann equation.[7] In this text, the authors argue that the electron-electron collision integral must be the dominant term in the electron Boltzmann equation if a Maxwellian speed distribution is to exist. An order of magnitude analysis is performed and the following partial list of conditions is derived:

$$\sum_h \frac{m_e}{m_h}\frac{\overline{\nu}_{eh}}{\overline{\nu}_{ee}} << 1 \tag{B1}$$

$$\frac{1}{\overline{\nu}_{ee}\tau} << 1 \tag{B2}$$

$$\frac{\overline{C}_e}{\overline{\nu}_{ee}L} << 1 \tag{B3}$$

$$\left(\frac{U_e}{\overline{C}_e}\right)^2 \frac{\overline{\nu}_{eH}}{\overline{\nu}_{ee}} << 1, \tag{B4}$$

where

$$U_e = \frac{-k}{m_e n_e}\frac{\nabla(n_e T)}{\overline{\nu}_{eh}},$$

$\overline{C}_e$ is the average electron speed; U_e the electron diffusion velocity; $\overline{\nu}_{eh}$ and $\overline{\nu}_{ee}$ the electron-heavy and electron-electron collision frequencies, and τ and L the characteristic time and length scales for macroscopic change. To evaluate these expressions, various assumptions must be made. It is assumed that the electron energy distribution is Maxwellian, so that the average electron speed can be calculated as $(8kT/\pi m_e)^{1/2}$. T is assumed to decrease from 8000 to 2500 K linearly over 65 cm such that $\Delta z/\Delta T \approx 1.2\times10^{-4}$ m/K, where z represents the distance from the nozzle exit. A 100 K temperature drop therefore occurs over 1.18×10^{-2} m. The product (n_eT) is evaluated at LTE conditions. Finally $\nabla(n_eT)$, evaluated over a drop in temperature of 100 K, can be approximated as $\Delta(n_eT)/\Delta z$ where $\Delta z = 1.2\times10^{-2}$ m. The collision frequencies are evaluated with equilibrium number densities and the electron collision cross sections found in Gupta.[2]

The first of these conditions results from the requirement that the electron-electron collision integral be much larger than the electron-heavy collision integral. The next two expressions assure that the plasma is collision-dominated with respect to the electron gas. They state that the time between electron-electron collisions is much less than the characteristic time scale for macroscopic change and that the mean free path for electron-electron collision is much smaller the characteristic length scale of macroscopic change. τ and L are taken as the time to traverse the longest test section (1.29 ms) and the length of this test section (0.65 m), respectively. The final condition requires that the term in the energy equation involving the electric field E' is small compared to the

electron-electron collision integral. Numerical evaluations of these conditions are shown in Fig. B1.

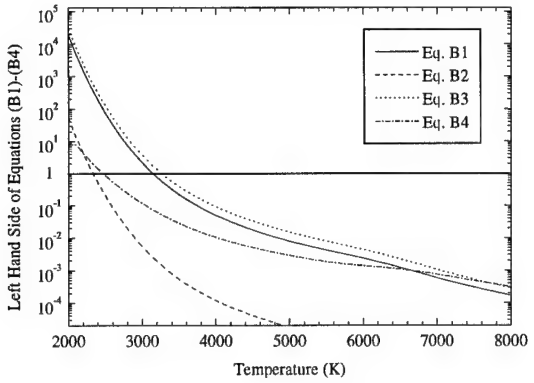

Figure B1. Evaluation of sufficient conditions for the existence of a Maxwellian electron energy distribution.

For temperatures less than ~3800 K, it appears that these sufficient conditions may be violated for an LTE air/argon plasma. It is possible that the observed non-LTE behavior of the air/argon experiments will delay a departure of the electron energy distribution from a Maxwellian. For example, the inferred ρ_e of ~500 at 65 cm (Fig. 28) would increase $\bar{\nu}_{ee}$ and thereby definitely prolong the validity of Eqs. B2 and B3, and possibly Eqs. B1 and B4 depending on the degree of chemical nonequilibrium. Considering both the approximate nature of these calculations and the fact that these conditions are sufficient but not necessary, a closer examination of the existence or lack of a Maxwellian distribution is justified.

5. Publications

5.1. Journal articles

Gessman, R.J., Laux, C.O., and Kruger, C.H., "Experimental Study of Kinetic Mechanisms of Recombining Atmospheric Pressure Air Plasmas," in preparation for AIAA Journal, 1997.

Laux, C.O., Gessman, R.J., and Kruger, C.H., "Experimental Study of a Recombining Nitrogen Plasma," in preparation for the AIAA Journal, 1997.

Levin, D.A., Laux, C.O, and Kruger, C.H., "A General Model for the Spectral Calculation of OH Radiation in the Ultraviolet," submitted to *JQRST*, 1997.

Kruger, C.H., Owano, T.G., and Laux, C.O., "Experimental Investigations of Atmospheric Pressure Nonequilibrium Plasma Chemistry," *IEEE Transactions on Plasma Sciences*, Vol. 25, No. 5, pp. 1042-1051, October 1997 (invited submission).

Laux, C.O., Gessman, R.J., and Kruger, C.H., "Ionizational Nonequilibrium Induced by Neutral Chemistry in Air Plasmas," *AIAA Journal,* Vol. 34, No. 8, pp. 1745-1747, 1996.

Sarrette, J.P., Gomès, A.M., Bacri, J., Laux, C.O., and Kruger, C.H., "Collisional-Radiative Modeling of Quasi-Thermal Air Plasmas with Electronic Temperatures Between 2000 and 13,000 K —I. $\Theta_e > 4000$ K," *JQSRT*, Vol. 53, No. 2, pp. 125-141, 1995.

5.2. Conferences and presentations

Laux, C.O., Gessman, R.J., Owano, T.G., and Kruger, C.H., "Experimental Investigation of Nonequilibrium Plasma Chemistry at Atmospheric Pressure," presented at the 13th International Symposium on Plasma Chemistry, Beijing, China, August 18-22, 1997.

Owano, T.G., Laux, C.O., and Kruger, C.H., "Experimental Investigation of Nonequilibrium Plasma Chemistry at Atmospheric Pressure," Proceedings of the 13th International Symposium on Plasma Chemistry, pp. 82-87, Beijing, China, August 18-22, 1997.

Kruger, C.H., Owano, T.G., Laux, C.O., and Zare, R.N., "Nonequilibrium in Thermal Plasmas," Proceedings of the 23rd International Conference on Phenomena in Ionized Gases, Toulouse, France, July 17-22, 1997 (invited).

Gessman, R.J., Laux, C.O., and Kruger, C.H., "Experimental Study of Kinetic Mechanisms of Recombining Atmospheric Pressure Air Plasmas," AIAA 97-2364, 28th Plasmadynamics and Lasers Conference, Atlanta, GA, June 23-25, 1997.

Candler, G.V., Laux, C.O., Gessman, R.J., and Kruger, C.H., "Numerical Simulation of a Nonequilibrium Nitrogen Plasma Experiment," AIAA 97-2365, 28th Plasmadynamics and Lasers Conference, June 23-25, Atlanta, GA, 1997.

Laux, C.O., Gessman, R.J., Hilbert, B., Packan, D.M., Pierrot, L.C., and Kruger, C.H., "Infrared Emission of Air Plasmas," Missile Signatures and Aerothermochemistry Meeting, Alexandria, VA, May 12-13, 1997.

Gessman, R.J., Laux, C.O., and Kruger, C.H., "Chemical and Ionizational Nonequilibrium in Recombining Atmospheric Pressure Air Plasmas," Gordon Research Conference on Plasma Processing Sciences, New Hampton, NH, August 11-16, 1996.

Laux, C.O., Gessman, R.J., and Kruger, C.H., "Radiative and Kinetic Studies of Nonequilibrium Air and Nitrogen Plasmas," Missile Signatures and Aerothermochemistry Meeting, NASA-Ames Research Center, April 22, 1996.

Laux, C.O., Gessman, R.J., Hilbert, B. and Kruger, C.H., "Infrared Signature Masking by Air Plasma Radiation," NASA-Ames Research Center, Computational Chemistry Seminar Series, April 10, 1996.

Gessman, R.J., Laux, C.O., and Kruger, C.H., "Mechanism for Ionizational Nonequilibrium in Air and Nitrogen Plasmas," Thermosciences Affiliates and Sponsors Conference, Stanford University, February 1996.

Laux, C.O., Gessman, R.J., and Kruger, C.H., "Radiative Phenomena in Nonequilibrium Plasmas," Mechanical Engineering Department Seminar, University of Minnesota, Minneapolis, MN, Nov. 20, 1995.

Michaud, F., Roux, F., Davis, S.P., Nguyen, A.-D., and Laux, C.O., "High-Resolution Fourier Spectrometry of the 14N2+ Ion for Optical Diagnostics in Air Plasmas," 14th Colloquium on High Resolution Molecular Spectroscopy, Dijon, France, Sept. 11-15, 1995.

Laux, C.O., Gessman, R.J., Hilbert, B., and Kruger C.H., "Kinetics and Radiative Studies of Air Plasmas," Computational Chemistry Seminar Series, NASA-Ames Research Center, Moffett Field, CA, August 30, 1995.

Laux, C.O., Gessman, R.J., and Kruger, C.H., "Ionizational Nonequilibrium in Thermal Air Plasmas," Proceedings of the 12th International Symposium on Plasma Chemistry, pp. 753-758, Minneapolis, MN, August 21-25, 1995.

Laux, C.O., Gessman, R.J., and Kruger, C.H., "Mechanisms of Ionizational Nonequilibrium in Air and Nitrogen Plasmas," AIAA Paper 95-1989, 26th AIAA Plasmadynamics and Lasers Conference, San Diego, CA, June 19-22, 1995.

Laux, C.O., Gessman, R.J., Hilbert, B. and Kruger, C.H., "Experimental Study and Modeling of Infrared Air Plasma Radiation," AIAA Paper 95-2124, 30th AIAA Thermophysics Conference, San Diego, CA, June 19-22, 1995.

Levin, D.A., Laux, C.O, and Kruger, C.H., "A General Model for the Spectral Calculation of OH Radiation in the Ultraviolet," AIAA 95-1990, 26th AIAA Plasmadynamics and Lasers Conference, San Diego, CA, June 19-22, 1995.

Laux, C.O., Gessman, R.J., and Kruger, C.H., "Experimental Studies and Modeling of Air Plasmas Produced in an ICP Torch," Missile Signatures and Aerothermochemistry Meeting, Space Dynamics Laboratory, Utah State University, Logan, Utah, April 7, 1994 (Invited).

6. Personnel

Professor Charles H. Kruger
Vice-Provost, Dean of Research and Graduate Policy,
Professor, Department of Mechanical Engineering.

Dr. Christophe O. Laux
Research Associate.
(Ph.D. Mechanical Engineering, Stanford University 1993).

Dr. Thomas G. Owano
Senior Research Associate.
(Ph.D. Mechanical Engineering, Stanford University 1991).

Dr. Laurent C. Pierrot
Postdoctoral Fellow
(Ph.D. Ecole Centrale Paris, 1997)

Mr. Richard J. Gessman
Graduate Research Assistant.
(M.S. Aeronautical and Astronautical Engineering, University of Illinois at Urbana-Champaign, 1992).

Mr. Benoit Hilbert
Graduate Research Assistant
(M.S. Mechanical Engineering, Stanford University, 1995).

Mr. Denis Packan
Graduate Research Assistant.
(M.S. Ecole Centrale Paris, France, 1996).

7. References

1. Dunn, M.G. and Kang, S.-W., "Theoretical and Experimental Studies of Reentry Plasmas," NASA, Report No. CR-2232, 1973.

2. Gupta, R.N., Yos, J.M., Thompson, R.A., and Lee, K.-P., "A Review of Reaction Rates and Thermodynamic and Transport Properties for an 11-Species Air Model for Chemical and Thermal Nonequilibrium Calculations to 30,000 K," NASA Report No. RP-1232, 1990.

3. Park, C., *Nonequilibrium Hypersonic Aerothermodynamics,* Wiley, New York, 1989.

4. Park, C., "Review of Chemical-Kinetic Problems of Future NASA Missions, I: Earth Entries," *Journal of Thermophysics and Heat Transfer*, **7,** 385-398, 1993.

5. Kee, R.J., Rupley, F.M., and Miller, J.A., "Chemkin-II: A Fortran Chemical Kinetics Package for the Analysis of Gas Phase Chemical Kinetics," Sandia National Laboratories, Report No. SAND89-8009, 1989.

6. Liu, Y. and Vinokur, M., "Equilibrium Gas Flow Computations. I. Accurate and Efficient Calculation of Equilibrium Gas Properties," *AIAA Paper 89-1736*, 1989.

7. Mitchner, M. and Kruger, C.H., *Partially Ionized Gases,* John Wiley & Sons, Inc., New York, 1973.

8. Sutton, G.W. and Sherman, A., *Engineering Magnetohydrodynamics,* McGraw-Hill, 1965.

9. Kruger, C.H., Owano, T.G., Gordon, M.H., and Laux, C.O., "Nonequilibrium Effects in Thermal Plasmas," *Pure and Applied Chemistry*, **64,** 607-613, 1992.

10. Laux, C.O., "Optical Diagnostics and Radiative Emission of Air Plasmas," Ph.D. Thesis, Stanford University, 1993.

11. Laux, C.O., Moreau, S., and Kruger, C.H., "Experimental Study and Improved Modeling of High-Temperature Air Radiation," *23rd AIAA Plasmadynamics and Lasers Conference, AIAA 92-2969*, Nashville, TN, 1992.

12. Laux, C.O., Gessman, R.J., and Kruger, C.H., "Modeling the UV and VUV Radiative Emission of High-Temperature Air," *28th AIAA Thermophysics Conference, AIAA 93-2802*, Orlando, FL, 1993.

13. Partridge, H., Langhoff, S.R., and Bauschlicher, C.W., "Theoretical Study of the A' $^5\Sigma_g^+$ and C" $^5\Pi_u$ States of N_2: Implications for the N_2 Afterglow," *Journal of Chemical Physics*, **88,** 3174-3186, 1988.

14. Park, C., "Calculation of Nonequilibrium Radiation in the Flight Regimes of Aeroassisted Orbital Transfer Vehicles", in *Thermal Design of Aeroassisted Orbital Transfer Vehicles*; *Vol. 96*, H. F. Nelson, Ed., American Institute of Aeronautics and Astronautics, 1985.

15. Park, C., "Nonequilibrium Air Radiation (NEQAIR) Program: User's Manual," NASA-Ames Research Center, Report No. NASA-TM86707, 1985.

16. Park, C., "Two-Temperature Interpretation of Dissociation Rate Data for N_2 and O_2," *26th Aerospace Sciences Meeting, AIAA 88-0458*, Reno, NV, 1988.

17. Candler, G.V., Laux, C.O., Gessman, R.J., and Kruger, C.H., "Numerical simulation of a nonequilibrium nitrogen plasma experiment," *28th AIAA Plasmadynamics and Lasers Conference, AIAA 97-2365*, Atlanta, GA, 1997.

18. Kruger, C.H., "Nonequilibrium effects in thermal plasma chemistry," *Plasma Chemistry and Plasma Processing*, **9,** 435-43, 1989.

19. Owano, T.G., Kruger, C.H., and Beddini, R.A., "Electron-ion three-body recombination coefficient of argon," *AIAA Journal*, **31,** 75-82, 1993.

20. Viggiano, A.A., Van Doren, J.M., Morris, R.A., and Paulson, J.F., "Evidence for an Influence of Rotational Energy on the Rate Constants for the Reaction Ar^+ ($^2P_{3/2}$) with N_2," *Journal of Chemical Physics*, **93,** 4761-1765, 1990.

21. Albritton, D.L., "Ion-Neutral Reaction Rates," *Atomic Data and Nuclear Data Tables*, **22,** 1, 1978.

22. Laux, C.O., Gessman, R.J., and Kruger, C.H., "Mechanisms of ionizational nonequilibrium in air and nitrogen plasmas," *26th AIAA Plasmadynamics and Lasers Conference, AIAA 95-1989*, San Diego, CA, 1995.

23. Levin, D.A., Laux, C.O., and Kruger, C.H., "A general model for the spectral calculation of OH radiation in the ultraviolet," *26th AIAA Plasmadynamics and Lasers Conference, AIAA 95-1990*, San Diego, CA, 1995.

24. Callear, A.B. and Pilling, M.J., "Fluorescence of Nitric Oxide. Part 6," *Transactions of the Faraday Society*, **66,** 1886, 1970.

25. Lahmani, F., Lardeux, C., and Solgadi, D., "Collision-induced relaxation of NO $C^2\Pi$ (v'=0) and $D^2\Sigma^+$ (v'=0)," *Chemical Physics Letters*, **81,** 531, 1981.

26. Laux, C.O., Gessman, R.J., and Kruger, C.H., "Ionizational Nonequilibrium Induced by Neutral Chemistry in Air Plasmas," *AIAA Journal*, **34,** 1745-1747, 1996.

27. Warnatz, J., "Rate Coefficients in the C/H/O System", in *Combustion Chemistry*, W. C. Gardiner, Jr., Ed., Springer-Verlag, New York, 1984.

28. Thielen, K. and Roth, P., "Resonance absorption measurements of N and O atoms in high temperature NO dissociation and formation kinetics," *Proc. 20th Symposium (International) on Combustion, 20*, (Combustion Institute), pp. 685, Ann Arbor, MI, 1984.

29. Tsang, W. and Herron, J.T., "Chemical kinetic data base for propellant combustion. I. Reactions involving NO, NO_2, HNO, HNO_2, HCN and N_2O," *Journal of Physical and Chemical Reference Data*, **20,** 609-663, 1991.

30. Mallard, W.G., Westley, F., Herron, J.T., and Hampson, R.F., "NIST Chemical Kinetics Database - Ver. 6.0," 1994.

31. Kossyi, I.A., Kostinsky, A.Y., Matveyev, A.A., and Silakov, V.P., "Kinetic Scheme of the Nonequilibrium Discharge in Nitrogen-Oxygen Mixtures," *Plasma Sources Science and Technology*, **1,** 207-220, 1992.

32. Gessman, R.J., Laux, C.O., and Kruger, C.H., "Experimental study of kinetic mechanisms of recombining atmospheric pressure air plasmas," *Proc. 28th AIAA Plasmadynamics and Lasers Conference, AIAA 97-2364*, Atlanta, GA, 1997.

33. Wilbers, A.T.M., Kroesen, G.M.W., Timmermans, C.J., Schram, D.C., "The continuum emission of an arc plasma," *JQSRT*, **45,** 1-10, 1991.

34. Biberman, L.M., Norman, G.E., and Ulyanov, K.N., "On the calculation of photoionization absorption in atomic gases," *Optics and Spectroscopy*, **10,** 297-299, 1961.

35. Gordon, M.H., "Nonequilibrium effects in a thermal plasma," Ph.D. Thesis, Stanford University, 1992.

36. Morris, J.C., Krey, R.U., and Garrison, R.L., "Bremsstrahlung and recombination radiation of neutral and ionized nitrogen," *Physical Review*, **180,** 167-183, 1969.

37. Riviere, P., Soufiani, A., Perrin, M.Y., Riad, H., and Gleizes, A., "Air mixture radiative property modelling in the temperature range 10,000-40,000 K," *JQSRT*, **56,** 29-45, 1996.